# Dimensional Tuning in Lead-Free Tin Halide Perovskite for Solar Cells

*Jinbo Zhao, Zuhong Zhang, Guixiang Li,* Mahmoud H. Aldamasy,* Meng Li,* and Antonio Abate*

**Due to its outstanding optoelectronic properties, halide perovskite solar cells (PSCs) power conversion efficiency has rapidly grown to 25.7%. Nonetheless, lead poisoning is a significant hurdle to the deployment of perovskite solar cells (PSCs). Tin is the most alternative with the most potential due to its similar electric and electronic properties to lead and its less hazardous nature. Yet, the performance of Sn-based PSCs lags significantly below that of Pb-based PSCs due to the Sn (II)'s easy oxidation to Sn (IV). Incorporating large-sized organic cations to form quasi-two-dimensional (2D) structured-tin perovskites increases the stability of the PSC. In addition, the hydrophobic group of the quasi-2D structure inhibits moisture and oxygen from penetrating the absorber layers. This review analyzes and evaluates the characteristics and performance of quasi-2D Sn-based perovskites such as Ruddlesden–Popper, Dion–Jacobson, and alternating cation interlayer (ACI). This work further proposes alternative strategies to improve the efficiency and stability of tin-based PSCs, including constructing new mixed 2D/3D perovskite structures, enhancing the transmission capacity, novel organic cations, and fabricating new ACI perovskite structures and controlling perovskite strain.**

## 1. Introduction

In recent decades, organic–inorganic hybrid halide perovskites have captivated the scientific community.[1] It demonstrated great potential in various optoelectronic applications such as solar cells, light-emitting diodes, and photodetectors.[2] The perovskite's general chemical formula is $ABX_3$, where A is an organic or inorganic cation, $FA^+$, $MA^+$, Cs, B is a metal ion such as $Sn^{2+}$, $Pb^{2+}$, $Ge^{2+}$, $Bi^{3+}$, and X is a halide anion as $Cl^-$, $Br^-$, or $I^-$.[3] Due to ideal photovoltaic properties such as the adjustable band gap, high carrier transport mobilities, long hole–electron diffusion lengths, and small exciton binding energies, the power conversion efficiency (PCE) of lead-based perovskite solar cells (PSCs) surged from 3.8% in 2009 to 25.7% in 2022.[4] However, lead toxicity and bioavailability have impeded the commercialization of lead-based PSCs, prompting researchers to seek an alternative.[5] The most common options to lead are $Sn^{2+}$, $Bi^{3+}$, $Ge^{2+}$, $Sb^{3+}$, and $Cu^{2+}$.[6] Theoretically, $Sn^{2+}$ is the most promising candidate to replace lead-based perovskites, demonstrating excellent photoelectric performance because Sn perovskite materials have a larger absorption spectrum in the visible range and a narrower optical band gap (1.3 eV) than Pb perovskite materials.[6e,7] This optimum bandgap enables tin-based PSCs to achieve a PCE of around 33% in theory.[8] Although the initial efficiencies of tin perovskites were poor,[9] the reported record is 14.8% in 2022.[3a,10] This demonstrates the potential of Tin as a perfect substitute for lead in PSCs. However, the PCE of Tin PSCs is still much lower than that of lead PSCs, which is mainly attributed to the two factors. First, the $Sn^{2+}$ easily becomes a stable $Sn^{4+}$ state in the air even in a nitrogen atmosphere, leading to the generation of many Sn vacancies, resulting in p-doping concentrations that could decrease the charge-carrier transfer. Moreover, fast crystallization is also the main factor hindering the improvement of Sn perovskite's performance. The 5p orbital of Sn has higher orbital energy than 6p of Pb, making 5p orbital of Sn exhibit stronger electrophilic ability than 6p of Pb, leading to the Lewis acidic. Thus, $SnI_2$ could easily react with Lewis bases, such as MAI and FAI, and show faster than $PbI_2$. According to the LaMer model, the fast nucleation rate would lead to poor-quality perovskite film with a high density

J. Zhao, Z. Zhang, M. Li
Key Lab for Special Functional Materials of Ministry of Education
National and Local Joint Engineering Research
Center for High-efficiency Display and Lighting Technology
School of Materials Science and Engineering
and Collaborative Innovation Center of Nano
Functional Materials and Applications
Henan University
Kaifeng 475004, China
E-mail: mengli@henu.edu.cn

G. Li, M. H. Aldamasy, M. Li, A. Abate
Helmholtz-Zentrum Berlin für Materialien und Energie
Kekuléstraße 5, 12489 Berlin, Germany
E-mail: guixiang.li@helmholtz-berlin.de;
mahmoud.hussein@helmholtz-berlin.de

A. Abate
Department of Chemical
Materials and Production Engineering
University of Naples Federico II
pzz.le Vincenzo Tecchio 80, 80125 Naples, Italy

The ORCID identification number(s) for the author(s) of this article can be found under https://doi.org/10.1002/aenm.202204233.

**DOI: 10.1002/aenm.202204233**

of defects.[11] That is why Sn perovskites are sensitive to oxygen and moisture, and their efficiency is poor.[8a,12] Researchers have tried various approaches to address these issues, including additive engineering with metallic Tin, $SnF_2$, $SnI_2$, reducing agents containing Lewis-based groups, hydrazine, and solvent engineering using DMF and DEF: DMPU, among others.[13] Despite these, tin PSCs still pronounce inferior stability.[14] Therefore, developing strategies to improve device stability is vital. Introducing large organic cations into tin perovskite's structure recently stabilized Sn perovskite materials and devices.[15] It is found that large organic cations do not incorporate into the perovskite crystal structure or even the lattice vacancies but form a quasi-two-dimensional (2D) perovskite. These cations benefit from hydrophobic organic groups that create low-dimensional perovskites, which improve stability dramatically.[16] Also, the 2D perovskite structures with low formation energy reduce ions migration and enhance stability.[17] Moreover, introducing organic cations leads to better band alignment and vertical growth of the perovskite films.

Quasi-2D perovskites include three types: Ruddlesden–Popper (RP), Dion-Jacobson (DJ),[18] and alternating cation interlayer (ACI).[19] The three structures originate from the same cutting direction. 3D perovskite slabs are separated by organic spacer cations interacting with the halide group ions in the perovskites.[20] The three types differ in interlayer materials,[21] interlayer distance,[22] and interlayer interaction.[23] Van der Waals gap between the long organic interlayer could improve the stability.[24] In addition, quasi-2D perovskites show better flexibility and hydrophobicity than 3D perovskite.[25] Such remarkable characteristics of quasi-2D structures can significantly decrease the formation of $V_{sn}$ to improve stability.[26]

In this study, we highlight recent advances in enhancing the stability of tin-based PSCs from the standpoint of crystal structure. We demonstrate the remarkable progress of RP, DJ, and ACI structures in Sn-based PSCs. Besides, we discuss the effects of 2D types on the properties of perovskite films. Due to the lack of reports on ACI-based tin perovskites, we highlight the research progress of ACI-based lead PSCs to motivate the tin PSCs research community. There have been some noteworthy accomplishments in these areas. However, numerous difficulties are ahead, including a better knowledge of the characteristics of quasi-2D tin perovskites and their applications. The progress of these structures is then reviewed, and recommendations for future growth are made.

## 2. Three-Dimensional Tin-Based Perovskites

3D perovskites are the typical and standard perovskite structures usually made and presented in the literature.[11c] $FASnI_3$ is the most classical 3D structure in the current reports, as shown in **Figure 1**a. 3D tin-based PSCs are spatial 3D structures with excellent carrier transport capacity.[27] Besides, it has low surface defect density, weak exciton combination energy,[28] high light absorption coefficient,[29] and high charge carrier mobility.[30] Tin perovskites attracted the researcher's attention very early. Knantzidis and co-workers[3a] reported a PCE of tin organic–inorganic hybrid PSCs of around 6%, implementing $CH_3NH_3SnI_{3-x}Br_x$ as a precursor and spiro-OMeTAD as a hole transport material (HTM). The device structure is shown in Figure 1b, and the experimental results demonstrated that the structure of the tin-based absorber material could be controllably tuned to cover most of the visible spectrum, showing a PCE of 5.73% in 2014. Concurrently, Snaith and co-workers[9a] first reported the $MASnI_3$ PSCs on a mesoporous $TiO_2$ scaffold. As a result, they obtained an open circuit voltage ($V_{OC}$) of over 0.88 V and a PCE of 6.4% from a 1.23 eV band gap material. To improve the PCE of tin perovskites, researchers followed different strategies such as the application optimization of different fabrication techniques of perovskite thin films (Figure 1c,d),[31] manipulating absorption layer structure (Figure 1e,f),[32] changing the device structure (regular and inverted), and architecture (mesoporous and planar).[14a,33] (Figure 1g).

## 3. Layered Two-Dimensional Tin-Based Perovskite

Tin-based PSCs have seen a significant rise in efficiency during the previous decade. However, the stability improvements were limited.[35] To increase the stability of tin perovskites, researchers try to introduce large organic cations that act as spacers and do not enter into the cubic structure.[14e] As a result, a new perovskite material called quasi-2D perovskite appeared. This structure showed better stability and retained the high efficiency reported earlier.[36] Thus, this structure provides a promising strategy for improving solar cell stability.[37]

### 3.1. Differences Between RP, DJ, and ACI

Although the three structural types are homologous, based on large organic cations incorporated between inorganic octahedral $[SnX_6]^{4-}$ layers, the differences are as follows:

#### *3.1.1. Architectural*

Firstly, the structural arrangement of organic spacers is different. The interlayer material of RP perovskite is a bilayer structure of monovalent cation pairs whose chemical formula is $A'_2A_{n-1}Sn_nX_{3n+1}$ (A′ is a monovalent organic cation with a relatively large ionic radius, and A is an organic cation). DJ perovskite is a monolayer structure of divalent organic cations with a chemical formula of $(A')(A)_{n-1}B_nX_{3n+1}$, where A′ is divalent interlayers of organic cations.[25] While the interlayer material of ACI perovskite is divalent-cations and a large-small alternating-cation interlayer, and the chemical formula is $(A')A_nB_nX_{3n+1}$, where A′ is a slightly larger cation such as $GA^+$ and the A is a smaller cation such as $MA^+$ (**Table 1**).[38]

Secondly, the interlayer spacing is also one of the differences between the three perovskites. The interlayer spacing of RP perovskite is 5.29 Å due to the monovalent cation pairs' bilayer structure.[39] The minimum interlayer spacing of DJ perovskite is 2 Å owing to the monolayer structures of those divalent organic cations.[40] For ACI perovskite, the interlayer spacing is between RP and DJ as 3 Å (Table 1).[22] Generally,

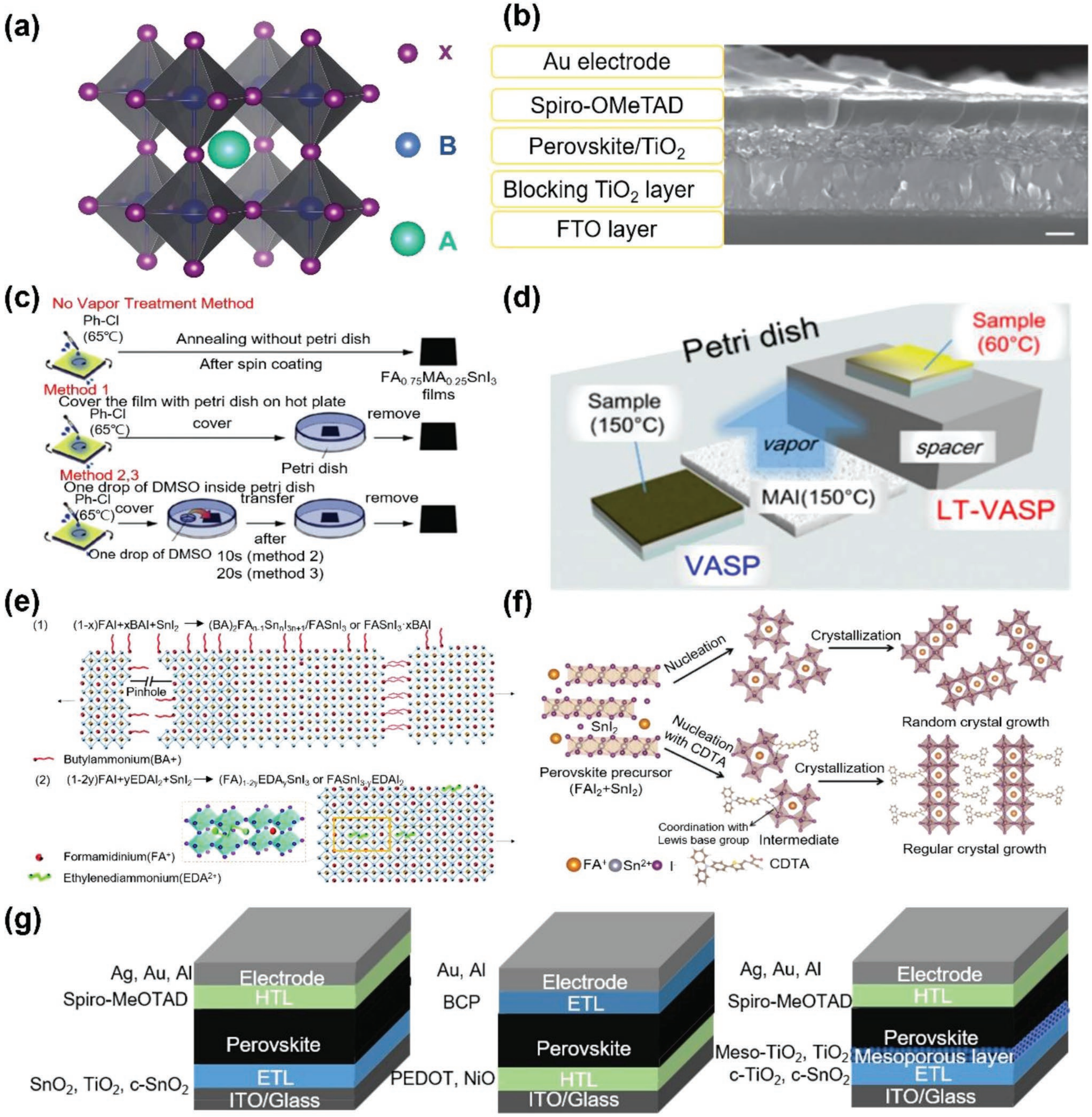

**Figure 1.** a) Perovskite lattice structure of 3D perovskites. b) Cross-sectional scanning electron microscope (SEM) images of intact photovoltaic devices of $CH_3NH_3SnI_3$ perovskite. Reproduced with permission.[3a] Copyright 2014, Nature Publishing Group. c,d) Different thin film fabrication methods. Reproduced with permission.[31] Copyright 2018, Wiley-VCH; Copyright 2016, American Chemical Society. e,f) Schematic diagram of structural changes of absorption layer in the presence of BAI, $EDAI_2$, and CDTA additives. Reproduced with permission.[34] Copyright 2018, Royal Chemical Society; Copyright 2019, Science China Press. g) Diagram for regular n-i-p, p-i-n, and mesoporous n-i-p structure.

with interlayer distances reduced, the photogenerated carrier dissociation degree of ACI perovskite becomes higher.

The third difference is the types of interlayer interaction. The interlayer interaction of RP perovskite is mainly Van der Waals gap and hydrogen bonding. The DJ perovskite eliminates the Van der Waals gap, leading to better stability.[41] The interlayer cations are only connected to the adjacent 2D perovskite plates by hydrogen bonds which enhance the interaction of inorganic layers (Table 1). As for ACI perovskite, since A and A′ alternate arrangement, hydrogen bonds and a weak Van der Waals gap existed.[18] The weakened Van der Waals force leads to the improved stability of ACI (**Figure 2**).[38b]

**Table 1.** Differences of three structures of Ruddlesden–Popper (RP), Dion–Jacobson (DJ), and alternating cation interlayer (ACI).

| | RP | DJ | ACI |
|---|---|---|---|
| Interlayer materials | Bilayer structure | Monolayer structures of divalent organic cations | Divalent-cation and alternating-cation interlayer |
| Minimum interlayer distance reported | 5.29 Å[39] | 2 Å[40] | 3 Å[22] |
| Types of interlayer interaction | Van der Waals gap + H bonding of monovalent cation | H bonding | Van der Waals gap (reduced) + H bonding large-small |
| Common long-chain spacer cations | Phenylethylammonium (PEA$^+$), butylammonium (BA$^+$), 5-ammoniumvaleric acid (5-AVA$^+$), formamide (FM$^+$), 2-thiopheneethylammonium (TEA$^+$), octylammonium (OA$^+$), dodecylammonium (DA$^+$), allylammonium (ALA$^+$) | 4-(Aminomethyl)piperidinium (4AMP$^{2+}$), 3-(aminomethyl)piperidinium (3AMP$^{2+}$), butyldiammonium (BEA$^{2+}$), 1,2-diaminoethane (EDA$^{2+}$), hexamethylenediamine (HDA$^{2+}$) | Guanidinium (GA$^+$), methylammonium (MA$^+$) |

### *3.1.2. Photoelectrical Properties*

As mentioned above, the three perovskites have different structures, leading to their different properties. RP perovskite intercalation is relatively weak van der Waals force, DJ, and ACI counterparts with strongly interacting hydrogen bonds, which lead to poorer stability than DJ and ACI perovskite. However, the dissociation energy of photogenerated carriers in DJ perovskite is larger.[42] GA$^+$ was introduced to make up ACI 2D perovskites with reduced hydrogen and van der Waals force.[19] This reduced the dissociation energy. Regarding adjacent distance, the DJ and ACI perovskites exhibit shorter distances than the RP perovskites. These could reduce quantum confinement and enhance the charge transfer of inorganic slabs.[43] The bandgap of 2D perovskites could be controlled by introducing different organic cations. For instance, the band gap of DJ perovskites with 3AMP$^{2+}$ is smaller than RP perovskites with BA$^+$.[9a] When a small volume of GA$^+$ was used to make up

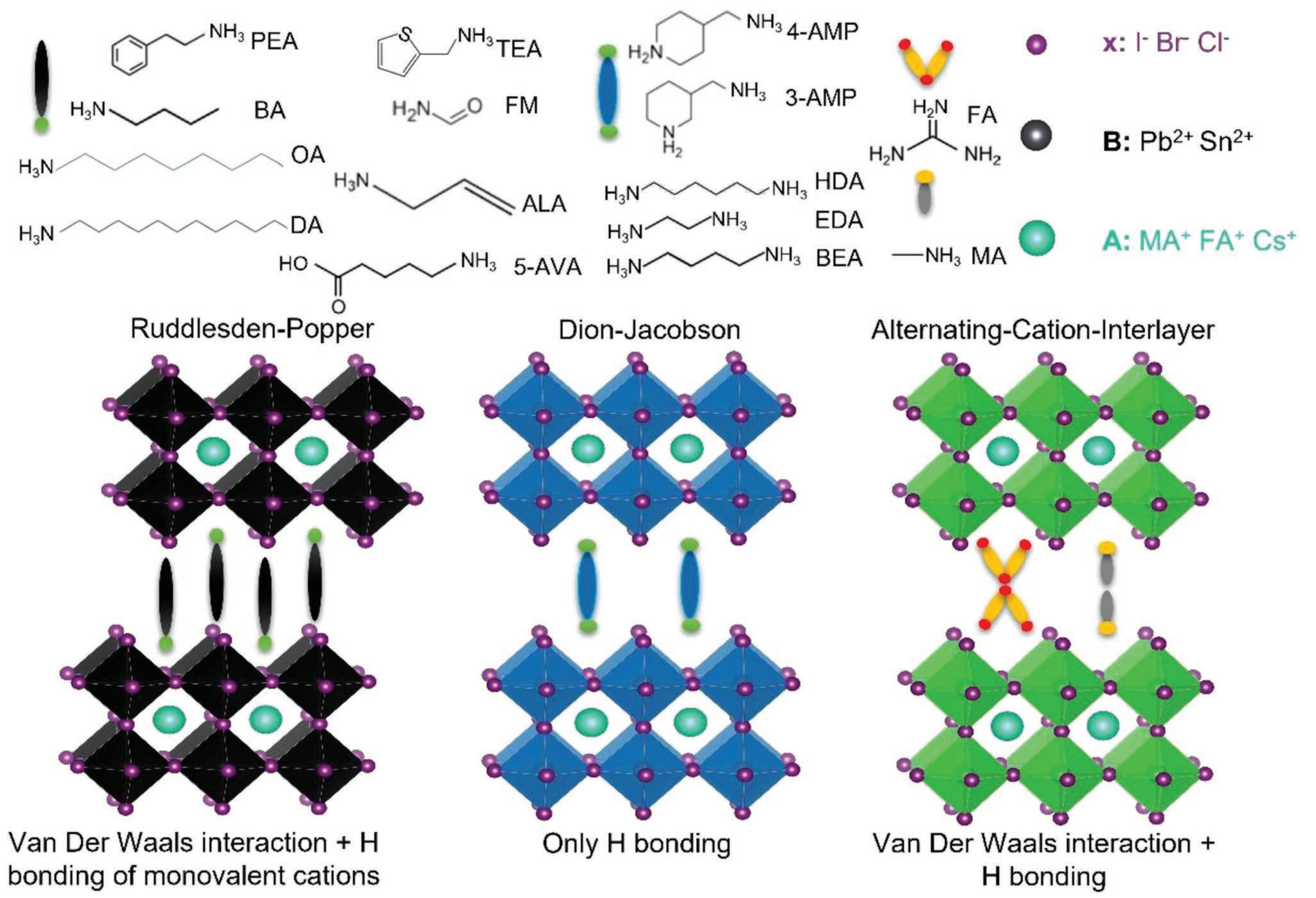

**Figure 2.** Comparison of three two-dimensional (2D) structures: RP (Ruddlesden–Popper), DJ (Dion–Jacobson), and ACI (Alternating-Cation-Interlayer).

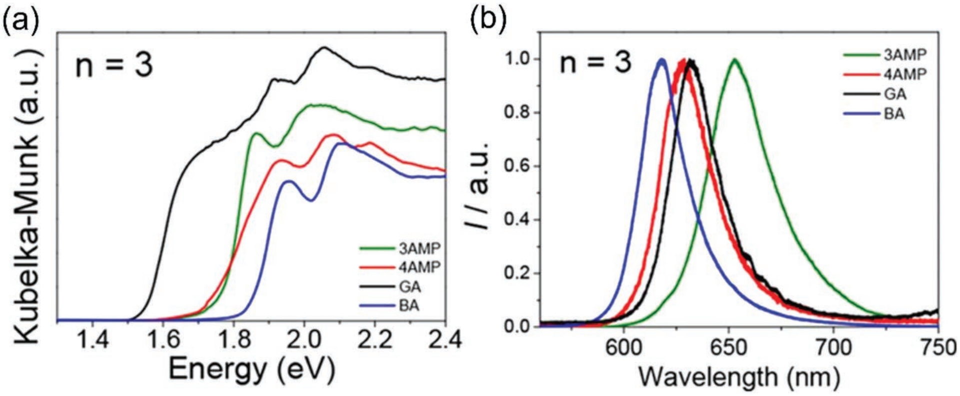

**Figure 3.** The comparison of a) optical absorption spectra. b) Photoluminescence (PL) spectra of 2D perovskites with different spacing groups. Reproduced with permission.[44] Copyright 2018, American Chemical Society.

ACI perovskite, a narrower bandgap is 1.73 eV was exhibited, as shown in **Figure 3**a.[44] Compared to DJ perovskite, the emission energy of BA counterparts blue-shifted by 0.1 eV (3AMP) and 0.03 eV (4AMP). The absorption edges of perovskite with $BA^+$ are 0.1 eV higher than the AMPs analog, as shown in Figure 3b.[44]

Although there was no report about ACI tin-based perovskite until this review was written, a higher degree of photogenerated carrier dissociation of ACI perovskite is worth researching. Based on the research progress of lead-based ACI perovskite analysis, fabricating the ACI tin-based PSC is an effective way of improving tin perovskite performance.

### 3.2. Ruddlesden–Popper Quasi-2D Sn Perovskite Solar Cells

To solve the stability problems of Sn-based PSCs, quasi-2D perovskite materials, such as $(BA)_2(MA)_{n-1}Pb_nI_{3n+1}$ series, have been developed, which show a tunable bandgap and high environmental stability.[20,45] Tin and lead have similar electronic properties, so 2D materials could be mutually applied to Tin and lead perovskites. 2D-RP tin perovskite chemical formula is $A'_2A_{n-1}Sn_nX_{3n+1}$ (A′ is a monovalent organic cation with a relatively large ionic radius, and A is an organic cation).[16a] 2D layered tin-based perovskite is a structure in which 3D perovskites are sliced and oriented along a specific crystallographic plane such as <100>, <110>, or <111>, and introduce bilayer large organic spacer cations to separate the inorganic octahedral slabs.[46] With <100>, orientation is the most common cutting direction. It is worth mentioning that charge balance supports the structural integrity of 2D perovskites and the organic spacer cations.[47] Cao and co-workers were the first to introduce butylammonium in tin perovskites ($(BA)_2(MA)_{n-1}Sn_nI_{3n+1}$) and obtained a PCE of 2.53%.[48] Surprisingly, the quasi-2D structure showed better temporal stability than 3D analogs, and the devices retained more than 90% of their initial efficiency after one month and only decreased to 50% after four months. To further explore the stability of 2D perovskites, Iwan Zimmermann and co-workers demonstrated that the smaller the band gap of 2D perovskites ($n < 4$), the better the solar cell performance.[49] However, the performance of 2D perovskite was still not satisfactory. We will discuss the advantage of low-dimensional Sn-based PSCs as follow:

#### *3.2.1. BA-Based Cations Ruddlesden–Popper Quasi-2D Sn Perovskite Solar Cells*

Due to the introduction of organic amine molecules in low-dimensional Sn perovskites could effectively regulate the crystallization process of perovskite films. Moreover, previous studies have shown that BA could react with perovskite to increase film stability. Thus, for a further understanding of 2D perovskites, Qiu and co-workers[50] studied the crystallization kinetics of quasi-2D tin perovskites by controlling the addition of Lewis adducts and monitoring the progress of ion exchange using a mixture of a polar aprotic solvent such as dimethyl sulfoxide (DMSO) and ion liquid solvent such as methylammonium acetate (MAAc) also known as L-I process. The perovskite structure was $BA_2MA_3Sn_4I_{13}$, where $n = 4$ (**Figure 4**a). By comparing the three pictures in Figure 4a, we observe that adding MAAc and DMSO as a co-solvent achieves dense and smooth $BA_2MA_3Sn_4I_{13}$ perovskite films with an average size of 9 µm. The devices fabricated by the L-I process showed a PCE of 4.03%, lower dark current density, higher carrier mobility, almost no hysteresis, and outstanding stability in the $N_2$ atmosphere for 94 days. In addition, Li and co-workers.[51] introduced ionic liquid *n*-butylammonium acetate (BAAc) to tune the $PEA^+$- and $EA^+$-based precursor coordination with solid O…Sn chelating bonds and N–H…X hydrogen bonds. These strong interactions effectively retarded the crystallization process and supplied more uniform nucleation sites (Figure 4b). Consequently, they obtained more compact quasi-2D perovskite films with preferential crystal orientation. Interestingly, introducing BAAc suppressed the $Sn^{2+}$ oxidation by DMSO and enhanced the film hydrophobicity and oxidation resistance. The resulting PSCs showed a PCE of up to 10.4%, and 96% of the initial efficiency was retained under ageing storage for over 1000 h. Impressively, they recorded device thermal stability at 85 °C, where 80% of the initial efficiency ($T_{80}$) over 400 h was demonstrated. This investigation reflects the high device stability enabled by the quasi-2D RP structure of Sn-based PSCs. To further improve the performance of quasi-2D RP Sn-based PSCs. Li and co-workers[52] studied the impact of different chain lengths on crystal orientation and phase distribution of quasi-2D tin perovskites by adding three additional spacers based on alkylamine cations, including butylamine ($BA^+$), octylamine ($OA^+$), and

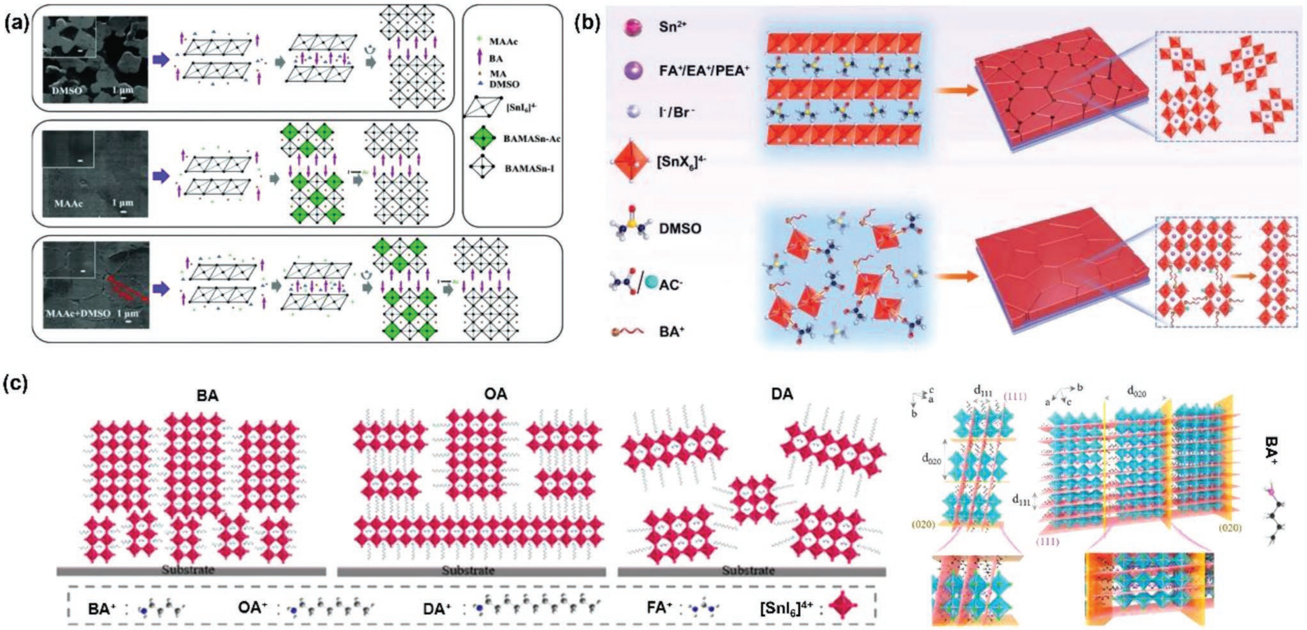

**Figure 4.** a) Scanning electron microscope (SEM) images and schematic diagram of the crystallization process of LDRP $BA_2MA_3Sn_4I_{13}$ perovskite films fabricated from different solvents: DMSO, MAAc, and DMSO + MAAc. Reproduced with permission.[50] Copyright 2019, Wiley-VCH. b) Schematic illustration of BAAc ionic liquid-assisted crystallization kinetics of Sn-based perovskite films. Perovskite films processed top is without and under is with BAAc. Reproduced with permission.[51] Copyright 2021, Wiley-VCH. c) Schematic illustration of crystal orientation, dimensionality, and phase distribution of 2D perovskite films: $BA^+$, $OA^+$, and $DA^+$. Reproduced with permission.[52] Copyright 2020, American Chemical Society.

dodecylamine ($DA^+$). The phase distribution of 2D tin perovskite crystals with shorter alkylamines was more ordered and oriented than with longer alkylamines (Figure 4c). Thus, the shorter alkyl chain in the organic spacer cations could retard the oxidation of $Sn^{2+}$ and induce crystal orientation growth and ordered phase distribution for better device performance. This study provides a perfect strategy for more stable PSCs fabrication.

In conclusion, BA based quasi-2D RP Sn-based PSCs have improved environmental stability and antioxidant properties compared to their 3D counterparts. Besides, compared to the longer chain organic space cations, BA exhibit the better performance in inducing the film vertical growth. Due to the quasi-2D RP perovskite film's low defect density, preferential crystal growth orientation, and transmission validity with BA introduction lead to PCE significantly increased.

### 3.2.2. PEA-Based Cations Ruddlesden–Popper Quasi-2D Sn Perovskite Solar Cells

PEA is also the first choice for building low-dimensional perovskite, which possesses a rigid benzene ring that could confine the structural freedom and stabilize the oriented structure leading to better perovskite film quality.[53] Liao and coworkers[54] prepared quasi-2D tin-based PSCs by introducing phenylethylammonium cation ($PEA^+$). They were the first to introduce $PEA^+$ into tin perovskites to form quasi-2D perovskite structures. They discovered that $PEA^+$ could enter the grain boundaries of perovskite, which reduces defects and direct the orientation of the growing perovskite crystals. As a result, the perovskite films were highly oriented, dense, and smooth, and a perpendicular growth was also obtained with a $FA^+$: $PEA^+$ ratio of 8:2 (**Figure 5**a). The quasi-2D $(PEA)_2(FA)_4Sn_5I_{16}$ perovskite delivered efficient charge carrier transport and showed a PCE of 5.94%. In addition, the device showed air stability for 100 h without any remarkable decay. Later, Chen and coworkers[55] introduced PEABr into the $FASnI_3$ perovskite film fabrication process. PEABr was spin-coated between the hole transport layer (PEDOT:PSS) and the absorption layer. They observed a thin layer of quasi-2D structures due to the steric effect (Figure 5b). The existence of a quasi-2D interlayer could promote the growth of perovskite crystals and reduce the hole traps by passivation. In addition, this work proved that the passivation effect produced by the quasi-2D structure could suppress the charge carrier's accumulation and recombination at the interface in Figure 5b. Consequently, a perovskite film with an improved morphology and reduced trap density was obtained and achieved a PCE of 7.05% without hysteresis.[56] Later, PEABr was applied to form a perovskite layer on the surface of the $FASnI_3$ and form an inverted quasi-2D structure.[57] Unlike Chen's work, PEABr bridge the electron transmission layer and perovskite film (Figure 5c). After the PEABr treatment, $Sn^{2+}$ oxidation was suppressed, defect density decreased, and band level alignment improved, which enhanced the $V_{OC}$ (Figure 5c). As a result, prepared devices showed a PCE of 7.86% and retained 80% of the initial PCE under light soaking for 350 h. Based on these results, $PEA^+$ was widely used in efficient quasi-2D tin PSCs to improve the performance of quasi-2D RP perovskites, where achieving vertically oriented growth of thin films is a practical advancement. Recently, Li and coworkers[58] used the phenyl ethylammonium chloride (PEACI)

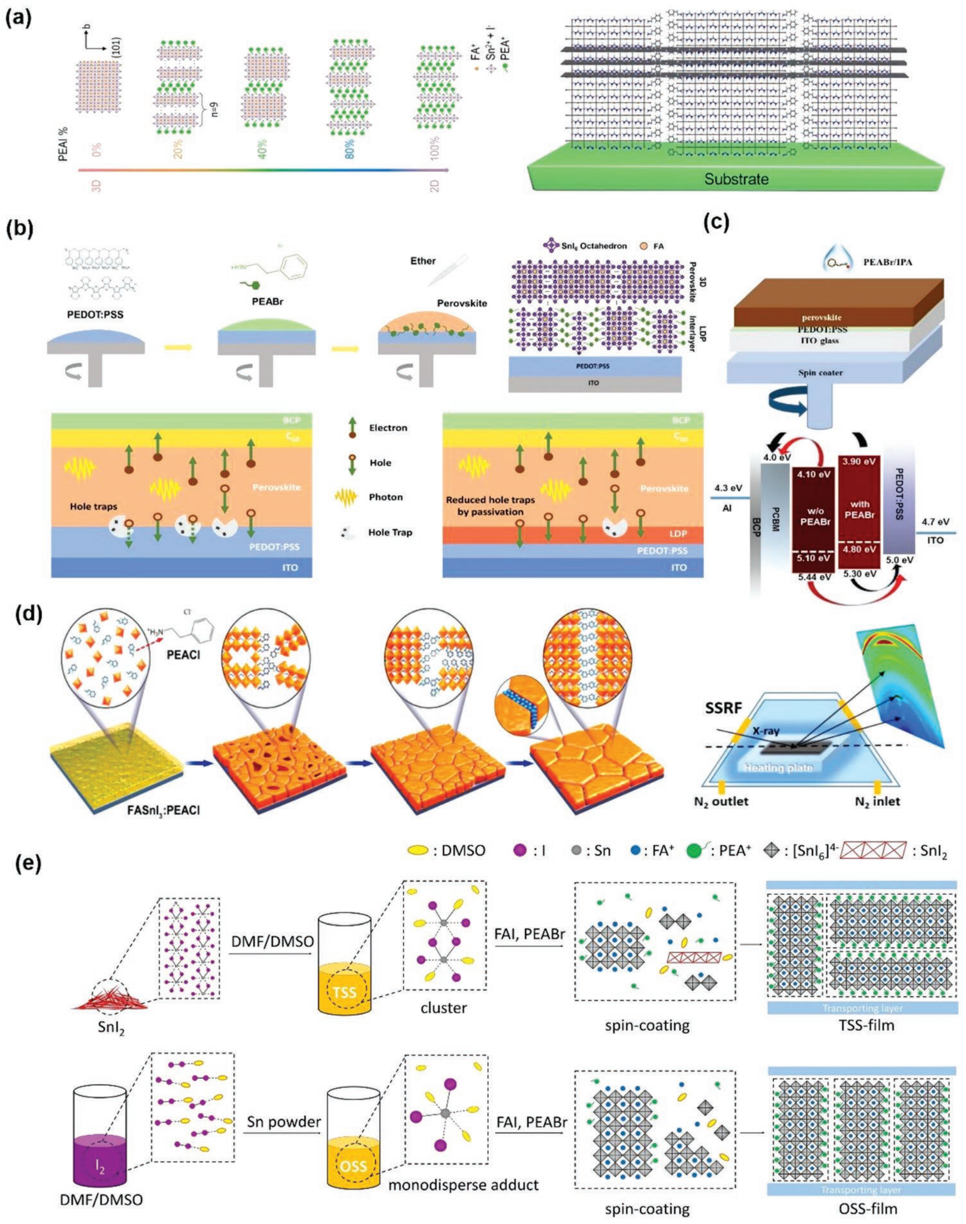

**Figure 5.** a) Structural diagram of tin perovskites with different concentrations of $PEA^+$ and the highly oriented perpendicular growth of the perovskite film with 20% $PEA^+$. Reproduced with permission.[54] Copyright 2017, American Chemical Society. b) Schematic diagrams of PEABr and illustration of PEABr treatment. The quasi-2D perovskite lattice formed between PEDOT:PSS and 3D perovskite after PEABr addition. Passivation process diagram of the low-dimensional structure formed after PEABr addition. Reproduced with permission.[55] Copyright 2018, Elsevier Ltd. c) Illustrative PEABr processing and energy level diagram of the inverted planar perovskite solar cells (PSCs) containing $FASnI_3$ without and with PEABr treatment. The energy level value of PCBM was obtained from a previous report. Reproduced with permission.[57] Copyright 2019, Wiley-VCH. d) Schematic diagram of crystal change of $FASnI_3$ and $FASnI_3$:PEACl films during different annealing temperatures. Simulation chart of high-resolution in situ synchrotron radiation test. Reproduced with permission.[58] Copyright 2020, American Chemical Society. e) Comparison of different synthetic routes: two-step synthesis and one-step synthesis. Reproduced with permission.[59] Copyright 2021, American Chemical Society.

as an additive to grow higher *n* value members of pure-phase quasi-2D crystals of tin perovskites. They could grow perovskite films with excellent vertical crystal orientation using assisted annealing of $FASnI_3$. As a result, highly crystalline, vertically oriented tin perovskite films were obtained. A barrier layer was formed at the surface of the crystals protecting the $Sn^{2+}$ from oxidation, which improved the film stability. Thus, the device got a PCE of 9.1% with a $V_{OC}$ of 0.59 V, $J_{SC}$ of 22.06 mA $cm^{-2}$, FF of 69%, and 1500 h of stability upon dark storage with almost no decrease in efficiency (Figure 5d). Ning and co-workers[59] have recently used the interaction between $I_2$ and DMSO to form $SnI_2\cdot(DMSO)_x$ complexes with enhanced coordination and PEABr as an additive. By comparison, it was found that $SnI_2$ could be well-dispersed into precursor solution and reduce

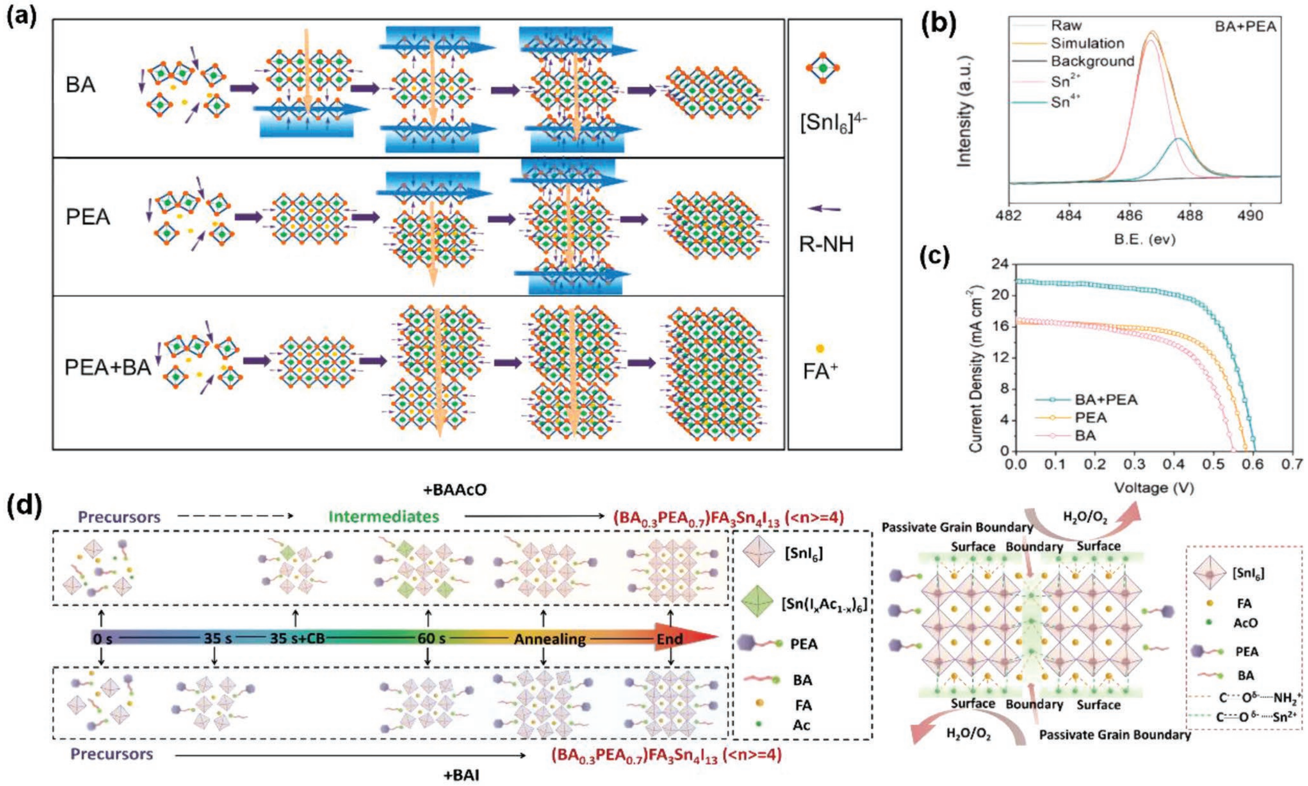

**Figure 6.** a) Schematic illustrations of the crystal growth process in two-dimensional (2D) Ruddlesden–Popper (RP) tin perovskites based on $BA^+$, $PEA^+$, and $PEA^+ + BA^+$. b) XPS spectra of 2D-RP tin perovskite films: $PEA^+ + BA^+$. c) *J–V* curves of 2D-RP tin perovskite devices based on $BA^+$, $PEA^+$, and $PEA^+ + BA^+$. a–c) Reproduced with permission.[60] Copyright 2019, American Chemical Society. d) Schematic diagram of the crystallization process of 2D-RP tin-based perovskites based on BAAcO and BAI. Reproduced with permission.[61] Copyright 2021, Science China Press.

the number of uncoordinated $SnI_2$. At the same time, highly coordinated $SnI_2 \cdot (DMSO)_x$ could guide out-of-plane crystal orientation and obtain more homogeneous perovskite films (Figure 5e). Compared to reference films, the electron diffusion length of Sn PSCs increased to about 80 nm, and the PCE was increased to 14.6%.

In conclusion, the introduction of PEA could improve the performance of quasi-2D Sn perovskite. The Ruddlesden–Popper quasi-2D Sn perovskite built by PEA could improve the crystallization process and structural stability and induce vertical-oriented film growth. Besides, the introduction of PEA leads to traps passivation and inhibition of carrier recombination. These all demonstrate the importance of PEA-based quasi-2D perovskite.

### 3.2.3. PEA and BA Mixture Ruddlesden–Popper Quasi-2D Sn Perovskite Solar Cells

PEA and BA are the two most widely used to build low-dimensional Sn perovskite, significantly promoting the development of low-dimensional Sn PSCs. In order to better improve the fast crystals and poor film quality of Sn perovskite, Qiu and co-workers[60] introduced $PEA^+$ and $BA^+$ to quasi-2D tin perovskites as mixed bulky organic cations to control the crystallization process. They found that the mixture suppressed the intermediate phase, enhanced homogeneity, and ordered crystal nucleation (**Figure 6**a). As a result, the $Sn^{4+}$ content was significantly reduced, which demonstrated that the oxidation of $Sn^{2+}$ was suppressed by adding $BA^+$ and $PEA^+$ together (Figure 6b). Moreover, scanning electron microscope (SEM) images showed a high-quality film formation with oriented crystal orientation. The PSCs showed an improved high PCE of 8.82% with a $V_{OC}$ of 0.6 V, $J_{SC}$ of 21.82 mA $cm^{-2}$, and FF of 66.73%. It is worth mentioning that using a single $BA^+$ or $PEA^+$ pronounced poor efficiency compared to adding both (Figure 6c). From the previously shown results, the mixture of $BA^+$ and $PEA^+$ effectively improved the performance. Qiu and co-workers[61] found that halide ions interact less with perovskite precursors solution and cannot control the complex crystallization process and the assembly of 2D-RP tin perovskite segments. Thus, they used a new ionic liquid bulky spacer, butylammonium acetate (BAAcO), to replace the traditional halide spacers BAI. They found that $AcO^-$ functional group strongly interacts with formamidinium ions ($FA^+$) and $Sn^{2+}$. These interactions could effectively control the crystallization process and protect the film surface from oxygen/water, passivate the grain boundaries (Figure 6d). Thus, a high-quality 2D-RP tin perovskites endowed with a narrow phase distribution and a highly vertical crystal orientation. As a result, they obtained a smooth, dense, and highly oriented perovskite film. The fabricated devices obtained a power conversion efficiency of 10.36% and retained 90% of the initial efficiency upon storage in $N_2$ for 600 h. The introduction of PEA and BA showing excellent film quality and device performance. These advances provide strategies for designing new types of additives in halide-free high-performance films.

### *3.2.4. Other Cations Ruddlesden–Popper Quasi-2D Sn Perovskite Solar Cells*

In order to fully understand the properties of quasi-2DRP structure and further improve the properties of tin-based perovskite, researchers have sought some new organic space cations. Chen and co-workers introduced another organic cation, 5-ammoniumvaleric acid (5-AVA$^+$ (AVA), to $FASnI_3$ ($n = 5$) and ammonium chloride ($NH_4Cl$) as an additive.[62] Generating highly vertically oriented films improved crystal quality and promoted carriers' separation and extraction. Thus, they obtained a PCE of 8.71%, and the initial efficiency was retained after 400 h without obvious decay. The work of Chen and co-workers laid a solid platform for high vertical perovskite crystal growth and conditions for enhancing the stability of tin PSCs (**Figure 7**a).[63] Sun and co-workers[64] reported formamide (FM) as a reducing organic cation into $FASnI_3$. The purpose of this molecule was to passivate defects and trap states such as undercoordinated tin atoms. During this process, $NH_2$ and C=O groups could interact with FA$^+$ and Sn$^{2+}$ to improve stability due to hydrogen bonding and Lewis acid-based coordination (Figure 7b). FM as a cross-linking agent (molecular glue), could change the grain growth direction, leading to enlarged grain size, enhanced crystallinity, and regular orientation. As a result, $FASnI_3$ with improved stability could retain 90% of the initial PCE when kept in an $N_2$ atmosphere for 8800 h. Xu and co-workers[65] used thiophene-based materials (TEAI) as the spacer cation in $MASnI_3$. Compared to pure $MASnI_3$, the quasi-2D perovskite films of 10% TEAI adding with high orientation and low content of Sn$^{4+}$ were formed (Figure 7c). This suggests that during the crystal grown process, the vertical growth orientation is stably controlled (Figure 7d).

That's all, quasi-2D RP Sn-based perovskite exhibit excellent stability and improved efficiency compared to the 3D analog. Adding different organic cations could adjust the properties of quasi-2DRP perovskite. According to the character of organic space cations, such as Lewis base reacts with $SnI_2$, reducing acid salt to improve the performance of Sn perovskite to control the crystallization and growth orientation to reduce defect density and enhance charge transmission. Their PCEs significantly increased because of the quasi-2D RP perovskite film's low defect density, flexible tunability, excellent crystal growth orientation, and transmission validity. The important previous works about quasi-2D RP tin-based PSCs were concluded in **Table 2**.

## 3.3. Dion–Jacobson Sn and Sn/Pb Mixture Perovskite Solar Cells

There are multiple structures in layered quasi-2D perovskites.[66] One of them is the Dion–Jacobson structure.[67] The

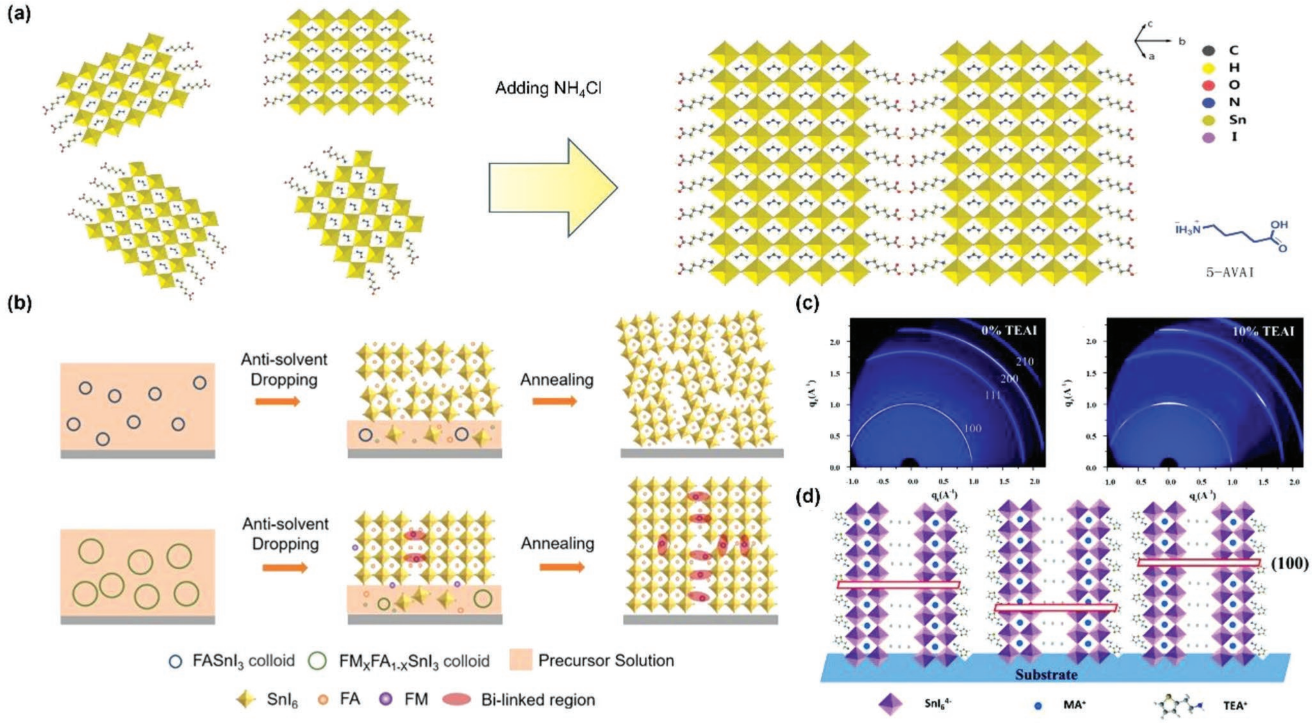

**Figure 7.** a) Diagram of the internal lattice of the $AVA_2FA_{n-1}Sn_nI_{3n+1}$ ($<n> = 5$) perovskite film after the addition of $NH_4Cl$. Reproduced with permission.[62a] Copyright 2019, Wiley-VCH. b) Schematic diagram of crystallization process after formamide (FM) addition. Reproduced with permission.[64] Copyright 2022, American Chemical Society. c) GIWAXS images of the (100) plane of $(TEA)_2(MA)_{n-1}Sn_nI_{3n+1}$with 10% TEAI. d) Schematic illustration of the (100) plane of $(TEA)_2(MA)_{n-1}Sn_nI_{3n+1}$with 10% TEAI. c,d) Reproduced with permission.[65] Copyright 2022, Royal Society of Chemistry.

**Table 2.** Summary of 2D Ruddlesden–Popper (RP) Sn-based perovskite photovoltaic parameters.

| Device structure | Device parameter | | | | Stability | Strategy | | Ref. |
|---|---|---|---|---|---|---|---|---|
| | PCE [%] | $J_{SC}$ [mA cm$^{-2}$] | $V_{OC}$ [V] | FF [%] | | | | |
| ITO/NiOx/$FASnI_3$/PCBM/Al | 5.94 | 14.44 | 0.59 | 69 | 100 h without delay | 20% $PEA^+$ | Crystal grown | 2017[54] |
| ITO/PEDOT:PSS/$MASnI_3$/PCBM/LiF/Al | 4.03 | 21.87 | 0.38 | 48.3 | 94 days in $N_{2,}$ no decrease | BA with MAAc | Crystallization kinetics | 2019[50] |
| ITO/PEDOT:PSS/$FASnI_3$/$C_{60/}$BCP/Cu | 7.05 | 24.87 | 0.45 | 63 | / | PEABr | Interface engineering | 2018[55] |
| ITO/PEDOT:PSS/$FASnI_3$/PCBM/BCP/Ag | 7.86 | 22.64 | 0.54 | 64 | With 80% PCE under light soaking for 350 h. | PEABr | Interface engineering | 2019[57] |
| ITO/c-$TiO_2$/m-$TiO_2$/$(BA)_2(MA)_{n-1}Sn_nI_{3n+1}$/PTAA/Au | 2.53 | 24.1 | 0.229 | 45.7 | 6.8% decay 30 d in $N_2$ | TEP | Crystal grown | 2017[48] |
| ITO/PEDOT:PSS/$FASnI_3$/PCBM/BCP/Ag | 7.71 | 20.69 | 0.54 | 69.06 | 90% of initial PCE in $N_2$ for 8800 h | FMI | Crystal grown | 2022[64] |
| ITO/PEDOT:PSS/Perovskite/Spiro-OMeTAD/Ag | 8.71 | 20.159 | 0.614 | 68.6 | 400 h without obvious decay in $N_2$ | $NH_4Cl$+5-$AVA^+$ | Crystal grown | 2019[62a] |
| ITO/PEDOT:PSS/$(BA_{0.5}PEA_{0.5})_2FA_3Sn_4I_{13}$/C60/LiF/Al | 8.82 | 21.82 | 0.6 | 66.73 | 60% of initial PCE in $N_2$ for 24 days | BA+PEA | Crystal grown | 2019[60] |
| FTO/PEDOT:PSS/$FASnI_3$/C60/BCP/Ag | 9.1 | 22.06 | 0.59 | 69 | 1500 h decay in $N_2$ | PEACI, Assisted annealing | Interface engineering | 2020[58] |
| ITO/PEDOT/$FASnI_3$/ICBA/BCP/Ag | 14.6 | 20.6 | 0.91 | 77.1 | 96% initial PCE 100-days an $N_2$ | Synthetic $SnI_2$ | Solvent engineering | 2021[59] |
| ITO/PEDOT:PSS/$(BA_{0.3}PEA_{0.7})_2FA_3Sn_4(I_{1-x}Ac_x)_{13}$/ICBA/LiF/Al | 10.36 | 23.33 | 0.65 | 68.56 | 90% initial PCE for 600 h in $N_2$ | BAAcO | Crystal grown | 2021[61] |
| ITO/PEDOT:PSS/$MASnI_3$/PC61BM/BCP/Ag | 6.8 | 19.8 | 0.53 | 65.1 | / | TEAI | Crystal grown | 2022[65] |
| FTO/PEDOT:PSS/$FASnI_3$/C60/BCP/Ag | 10.4 | 22.2 | 0.65 | 71.6 | 96% initial PCE, 1000 h in $N_2$ | BAAc, EABr | Crystal grown | 2021[51] |

corresponding structure formula is $(A')(A)_{n-1}B_nX_{3n+1}$, where A′ is divalent interlayers of organic cations.[3b] The DJ perovskite belongs to cutting at the (100) plane of the oriented perovskite.[68] The difference between RP and DJ perovskites is that the interlayers of organic cations are monovalent and divalent, respectively.[67b,69] The spacer layer in the RP phase forms a van der Waals gap, bonds, and a small number of hydrogen bonds using bilayer organic cations (**Figure** 8a).[70] The DJ perovskite spacer layers with H bonds are directly connected to the adjacent perovskite slabs by monolayer bivalent organic cations (Figure 8b). This connection enhances the interaction force and causes the interlayer distance of DJ perovskite to be smaller than RP perovskite, which benefits the charge transfer of quasi-2D perovskite devices.[71] Also, DJ perovskites have less lattice distortion than the RP type, leading to better optoelectrical performance.[72] Therefore, DJ perovskites possess better stability compared to RP perovskites.[73]

### *3.3.1. Benzene-Based Sn Dion–Jacobson Perovskite Solar Cells*

To understand the characteristics of DJ tin perovskites, Chen and co-workers[74] introduced 4-(aminomethyl)piperidinium to form 2D-DJ perovskites.[44] The DJ structure of (4AMP)(FA)$_{n-1}Sn_nI_{3n+1}$ 2D-DJ perovskite is illustrated in Figure 8c. They surprisingly found that photoluminescence (PL) lifetime is as long as 18.56 ns, which is longer than most of the reported Sn-based PSCs and shows an optical bandgap of 1.47 eV in the PL spectrum. Besides, they investigated the *n* value of the perovskite material. The *n* value increases from 1 to 4, leading to a systematic red-shift of the absorption edge and PL peak. As the first successful preparation of 2D-DJ tin-based PSCs, it has no hole transporting layer and obtained a PCE of 4.22% with $J_{SC}$ of 14.90 mA cm$^{-2}$, $V_{OC}$ of 0.64 V, and FF of 0.443. The device was exposed to 1 sun illumination in an $N_2$ atmosphere at 45 °C for 100 h, and the initial PCE only decreased by 9%, demonstrating the stability of the device and providing the feasibility of developing DJ perovskite.[76] Later, Chen and co-workers[75] continued to explore the performance of DJ tin-based PSCs with 4AMP and found that the optimum dosage is 15 mol% $4AMP^{2+}$. This work added a hole transport layer to the PSCs structure compared to the previous experiment.[9b] On most of the optimum film surfaces, they found that many 4AMP are on the surface of $FASnI_3$. The 4AMP molecules could effectively passivate the grain surface and grain boundaries. They will have a great affinity with the Sn perovskite lattice, leading to a near-full-coverage functionalization, as shown in Figure 8d. This structure not only allowed a delay of $O_2/H_2O$ entering the bulk of the perovskite film, which improved stability but mitigated Sn defects for reduced nonradiative recombination of photocarriers. Thus, they obtained a PCE of 10.86%,

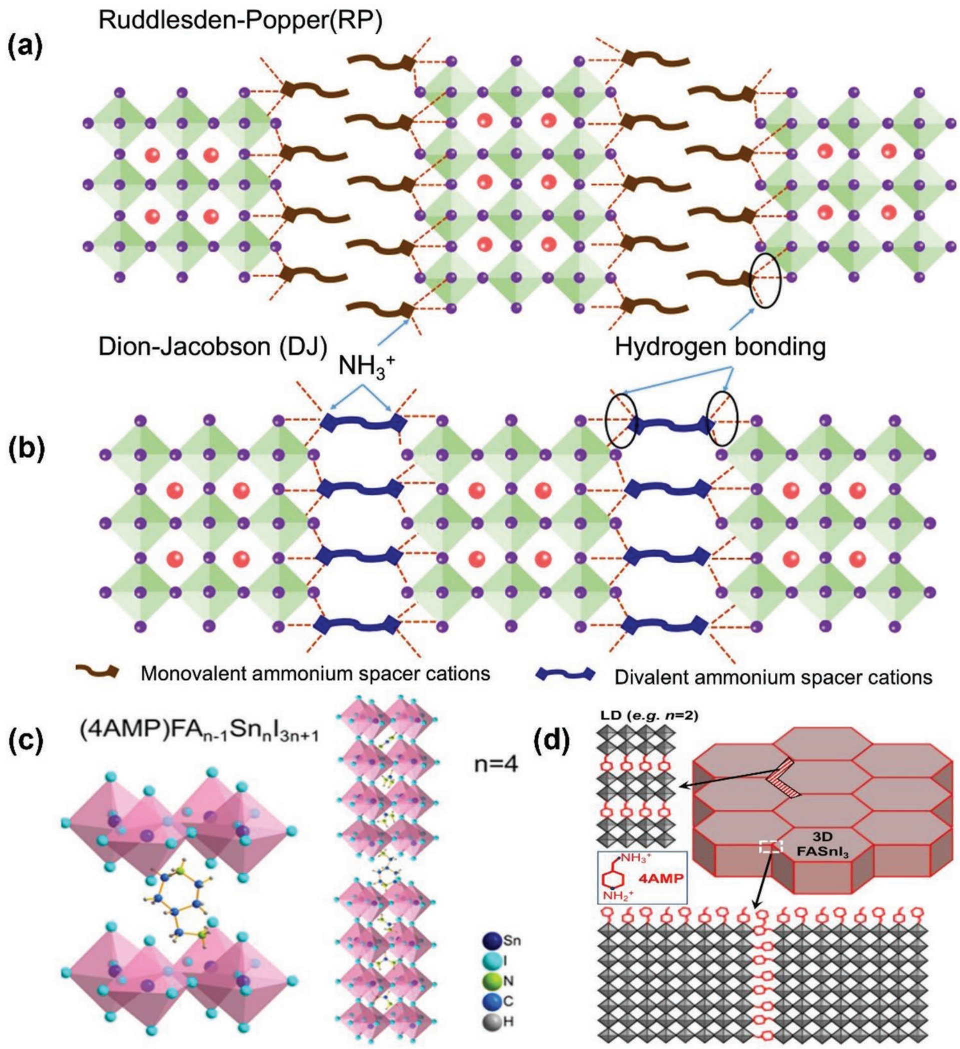

**Figure 8.** a) The structure of Ruddlesden–Popper (RP) perovskites. b) The structure of Dion–Jacobson (DJ) perovskites $n = 3$. a,b) Reproduced with permission.[70] Copyright 2019, American Chemical Society. c) DJ Sn-based halide perovskite $(4AMP)(FA)_{n-1}Sn_nI_{3n+1}$ ($n = 4$). Reproduced with permission.[74] Copyright 2018, American Chemical Society. d) Schematic illustration of the optimal functionalization of the grain surface and grain boundaries of the $FASnI_3$ perovskite polycrystalline thin film when 4AMP was added at 15 mol%. Reproduced with permission.[75] Copyright 2020, American Chemical Society.

and the original stable efficiency of 77% is maintained under continuous 1-sun illumination. The DJ Sn perovskite with 4AMP introduction could efficiently suppress trap generation, reduce nonradiative recombination, and increase light stability. This study played a guiding role in 2D-DJ Sn-based perovskite research.

### *3.3.2. Long Chain-Based Dion–Jacobson Sn Perovskite Solar Cells*

Although the PCE of DJ perovskite has advanced rapidly, its stability is not satisfactory. This point is worth exploring by researchers. Li and co-workers[76] introduced 1,4-butanediamine ($BEA^+$) to $FASnI_3$ (**Figure 9**a) to form DJ perovskite for improved stability. Due to the high crystal symmetry of (BEA), $FA_2Sn_3I_{10}$ has good absorption and carrier separation. With adding $BEA^+$, a low-dimensional DJ perovskite was formed, which suppressed the $Sn^{2+}$ oxidation. The densely formed perovskite films weakened the quantum confinement, improved carrier diffusion, and mobility, and created a barrier-free charge transport pathway. Thus, they achieved a stable perovskite film without hysteresis. Most importantly, the device exhibited remarkable stability and lost only 9% of its initial PCE after 1000 h of storage in an $N_2$ atmosphere without encapsulation. This work demonstrated the significance of $BEA^+$ in preparing stable hydrophobic 2D-DJ structures and provided the possibility for commercialization. Later, Ma and co-workers[77] investigated the passivation of crystal defects that benefited from DJ structures. They studied hexamethylenediamine diiodide (HDADI) as an organic cationic salt and introduced it into $FASnI_3$ precursor solutions (Figure 9b). The HDADI introduced into $FASnI_3$ controls nucleation and crystal growth kinetic process. The amino group of $HDA^{2+}$ could interact with the iodide of $[SnI_6]^{4-}$ forming a hydrogen bond, which facilitates the connection with

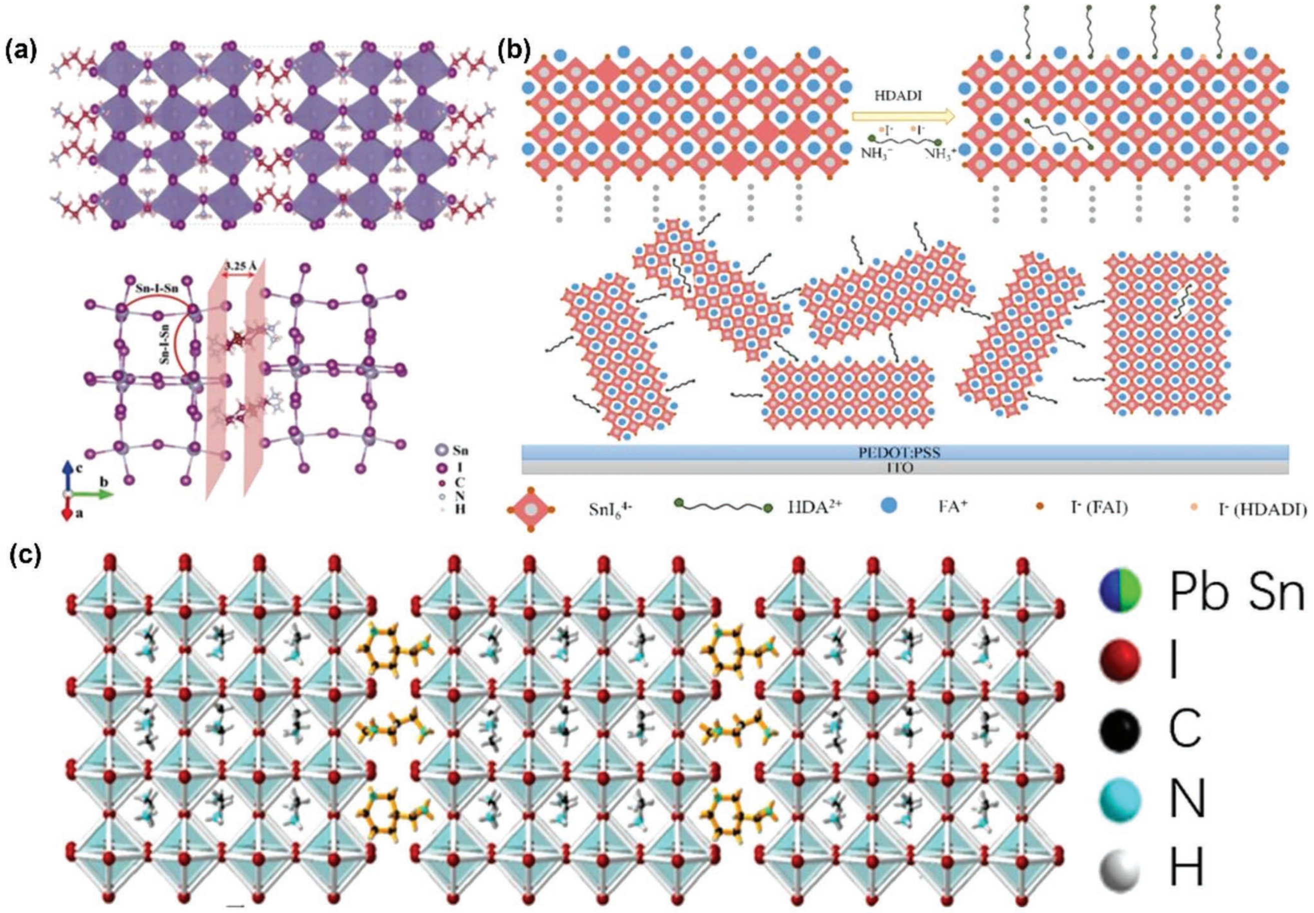

**Figure 9.** Schematic diagram of a) Lattice structure diagram with BEA$^+$ additive. Reproduced with permission.[76] Copyright 2020, Wiley-VCH. b) The internal reaction of $FASnI_3$ perovskite in the presence of hexamethylenediamine diiodide (HDADI) additive; Reproduced with permission.[77] Copyright 2020, American Chemical Society. c) Schematic diagram of two-dimensional (2D) Dion–Jacobson (DJ) phase perovskite $(3AMP)(MA_{0.5}FA_{0.5})_3(Pb_{0.5}Sn_{0.5})_4I_{13}$ ($n = 4$) prepared after the introduction of 3AMP. Reproduced with permission.[78] Copyright 2020, American Chemical Society.

perovskites to make up DJ perovskite (Figure 9b). Additionally, this reaction neutralized charged defects or dangling bonds and formed a barrier layer to suppress $Sn^{2+}$ oxidation to $Sn^{4+}$ and reduce $V_{sn}$. Thus, this work achieved a high-quality perovskite film with large film coverage, high crystallinity, and improved stability, which showed a PCE of 7.6% and remained at 80% of the initial efficiency in the $N_2$ environment for 550 h.

### 3.3.3. Dion–Jacobson Sn/Pb Mixture Perovskite Solar Cells

Recently, Ke and co-workers[78] combined the advantages of 2D DJ phases and Pb and Sn perovskite bandgap characteristics to form narrow bandgap PSCs. In addition, introducing 3-(aminomethyl)piperidinium ($3AMP^{2+}$) as an organic spacer cations, which led to the formation of 2D DJ perovskites $(3AMP)(MA_{0.5}FA_{0.5})_{n-1}(Pb_{0.5}Sn_{0.5})_nI_{3n+1}$ ($n = 4$) (Figure 9c). The bandgap of the prepared perovskite was 1.27 eV, which was lower than pure $(3AMP)(MA_{0.5}FA_{0.5})_{n-1}Sn_nI_{3n+1}$ ($n = 4$) (1.32 eV) and $(3AMP)(MA_{0.5}FA_{0.5})_{n-1}Pb_nI_{3n+1}$ ($n = 4$) (1.53 eV). Therefore, a PCE of 20.09% with a $V_{OC}$ of 0.88 V and 79.74% FF was obtained. The improved PCE demonstrated reduced nonradiative recombination due to the lower dark current and the higher carrier lifetime. This research provided viable strategies for improved DJ perovskite performance.

Two types of organic cations currently make up quasi-2DDJ Sn-based perovskites: Benzene-based and long-chain. These cations could interact with the iodide of $[SnI_6]^{4-}$ forming a hydrogen bond that leads to a more stable perovskite structure and contributes to defects suppression. Besides, DJ phase perovskite structure also applies to Sn–Pb perovskite with excellent performance, such as reduced nonradiative recombination and long-term stability. The important previous works about quasi-2D DJ tin-based PSCs were concluded in **Table 3**.

### 3.4. Alternating Cation Interlayer Perovskites and Their Potential for Sn PSCs

RP and DJ perovskites were extensively researched as low-dimensional perovskites.[68b] However, there are no reports about alternating cation interlayer (ACI) tin perovskites. As

**Table 3.** Summary of 2D Dion–Jacobson (DJ) perovskite photovoltaic parameters.

| Device structure | Device parameter | | | | Stability | Strategy | | Ref. |
|---|---|---|---|---|---|---|---|---|
| | PCE [%] | $J_{SC}$ [mA cm$^{-2}$] | $V_{OC}$ [V] | FF [%] | | | | |
| FTO/c-TiO$_2$/m-TiO$_2$/ZrO$_2$/(4AMP) FA$_3$Sn$_4$I$_{13}$/C | 4.22 | 14.9 | 0.64 | 44.3 | 9% decays 100 h in N$_2$(45 °C) | 4AMP | Crystal grown | 2018[74] |
| FTO/Cu-NiO$_x$/(4AMP)FA$_3$Sn$_4$I$_{13}$/PCBM/BCP/Ag | 10.9 | 21.15 | 0.69 | 74 | 77% initial PCE 500 h 1-sun illumination in N$_2$ | 4AMP | Interface engineering | 2020[75] |
| ITO/PEDOT:PSS/(BEA) FA$_2$Sn$_3$I$_{10}$/PCBM/Ag | 6.43 | 18.85 | 0.62 | 56.1 | 90% initial PCE after 1000 h in N$_2$ | BEA, Liquid phase crystallisation | Crystal grown | 2020[76] |
| ITO/PEDOT:PSS/FASnI$_3$/C60/BCP/Ag | 7.6 | 21.46 | 0.514 | 68.87 | 80% of the initial PCE 550 h in N$_2$ | HDADI | Crystal grown | 2020[77] |
| ITO/PEDOT/(3AMP) (MA$_{0.5}$FA$_{0.5}$)$_3$(Pb$_{0.5}$Sn$_{0.5}$)$_4$I$_{13}$ | 20.09 | 28.63 | 0.88 | 79.74 | 73.2% initial PCE 100 h 1-sun illumination in N$_2$ | Pb-Sn | Crystal grown | 2020[78] |

one of the perovskites cut along the (100) direction, the properties of ACI perovskites are similar to the other two (RP and DJ), whose formula is $A'A_nB_nX_{3n+1}$.[79] The A and the large A′ cations fill alternately between the perovskite layers. The layer superposition characteristics of the DJ structure and RP structure are adopted.[87] Compared with the RP perovskites, ACI perovskite exhibits high crystal symmetry and a narrower optical gap that could enhance absorption capacity.[19] ACI perovskite has lower exciton binding energy and longer carrier lifetime than RP perovskite due to the limited amount of GA and MA (GA = guanidinium, MA = methylammonium) as A-site ions. The peculiarities of the ACI structure have piqued scholars' interest.

In this context, we will introduce lead-based ACI perovskites to provide references for potential ACI tin perovskites, considering that tin perovskites were not reported and have the same properties as lead perovskites. Seo and co-workers first proposed ACI perovskites. The ACI $GAMA_3Pb_3I_{10}$ structure was formed and delivered a PCE of 7.26%.[22] They found that the smaller dielectric confinement of quantum wells (QWs) in the ACI structure would lead to a lower exciton binding energy than RP perovskite with the same $n$ value. Later, Gu and co-workers[80] studied the crystal dynamics of ACI perovskites and confirmed that ACI carriers are easy to separate. Obtained high stability and a more than 16% PCE and maintained 80% of its initial PCE after 2400 h of glove box storage.

Later, Zhao and co-workers[38a] used a solvent mixture of DMSO:DMF (1:10 v/v) as the solvent and introduced GA$^+$ to form ACI perovskite of $(GA)(MA)_nPb_nI_{3n+1}$ ($\langle n \rangle = 3$). They used antisolvent engineering and hot-casting techniques to control the kinetic transformation from disordered sol–gel colloidal precursor to the crystalline phase. The analysis of in situ GIWAXS demonstrated the formation of the intermediate crystalline solvate and the 2D $GA_2PbI_4$ perovskite (**Figure 10**a). Understanding the properties of the film, such as using QWs, improves introduced the MACI to control the quality of ACI perovskite. The results show a larger grain size, a smoother surface, and better crystalline quality of ACI films. Furthermore, the modified films enhanced photocurrent transport extraction between the QWs and suppressed the nonradiative charge recombination. As a result, the PCE improved significantly from 15.79% to 18.48%.[81] Moreover, Zhao and co-workers studied how the solvent effect influences the formation of ACI perovskite QWs. QWs formation was investigated by comparing whether DMSO was used as the additive solvent (Figure 10b). DMSO has a higher viscosity, resulting in a decreased solvent volatilization rate, leading to slower

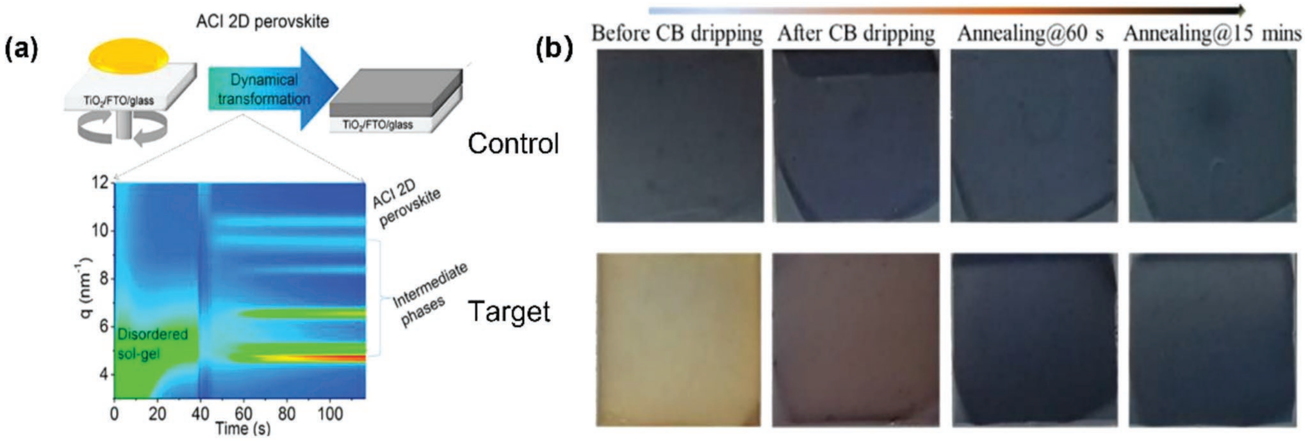

**Figure 10.** a) Alternating cation interlayer (ACI) perovskite formation process and in situ GIWAXS test figure Reproduced with permission.[38a] Copyright 2019, American Chemical Society. b) ACI films' surface morphology at different crystallization periods under other solvent conditions. Reproduced with permission.[82] Copyright 2021, Wiley-VCH.

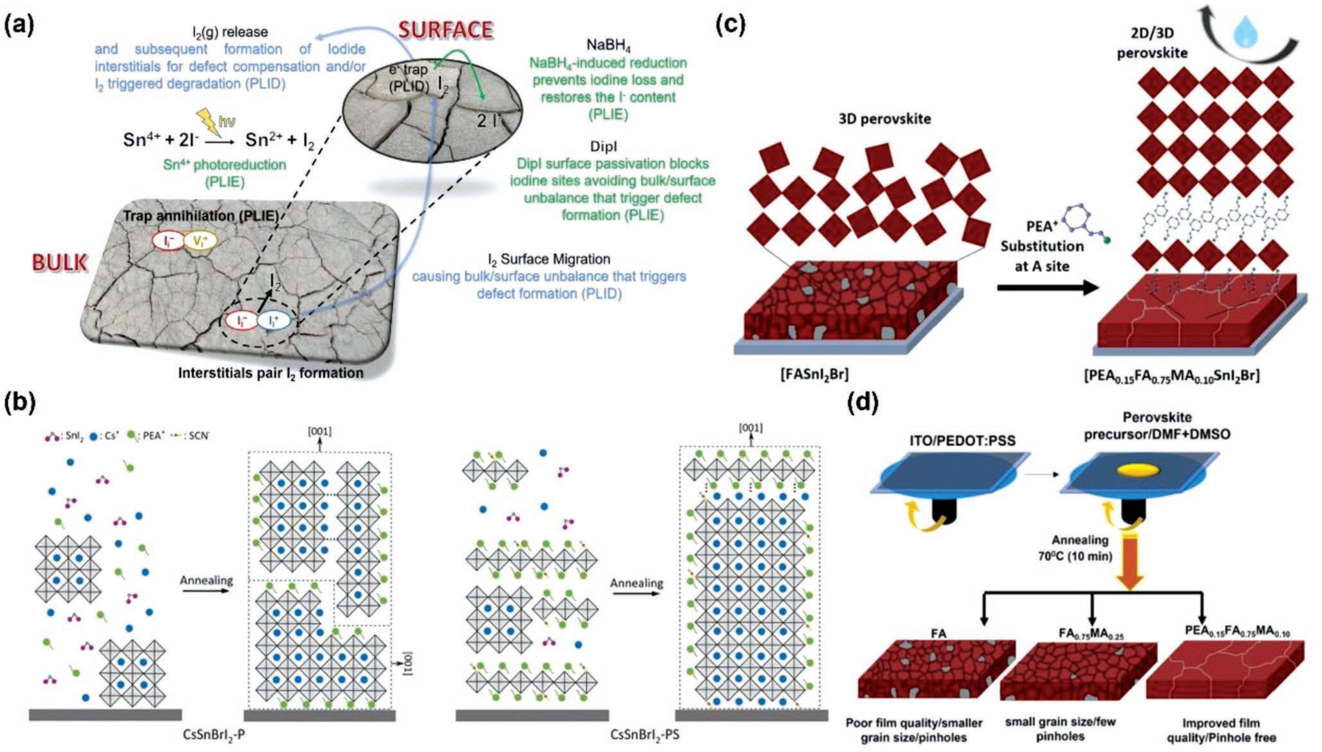

**Figure 11.** a) Schematic diagram of the internal reaction of the tin-based film under illumination. Reproduced with permission.[87] Copyright 2022, The Authors. Published by Elsevier Inc. b) Schematic comparison of crystallization mechanism between $CsSnBrI_2$-P and $CsSnBrI_2$-PS. Reproduced with permission.[86] Copyright 2021, Wiley-VCH. c) Schematic diagram of action mechanism of PEA⁺. d) Schematic diagram of the preparation of perovskite thin films and how to regulate the influence of A-site cations in the film growth process. c,d) Reproduced with permission.[88] Copyright 2022, Elsevier B.V.

crystallizations, showing that a better-quality film was obtained after adding DMSO. These improved efficient carrier charge transport and extraction and suppressed charge nonradiative recombination.[82] In addition, there are also some other additives to form ACI perovskites, such as PEA⁺.[83] By reviewing these lead-based ACI perovskites with delightful effects, we briefly understand the critical role of ACI structure in PSCs.

These examples demonstrated that quasi-2D ACI perovskite has excellent potential in Sn perovskite. For ACI, perovskite has a narrow band gap and shorter interlayer distance leading to enhanced charge transport. Moreover, reduced van der Waals gap could improve stability. These studies provide strategies for the research and development of tin-based ACI perovskites.

## 4. 2D/3D Heterojunction Tin-Based Perovskite

The introduction of large organic cations into perovskite precursors forms 2D perovskite structures, proving its resistance to moisture and oxygen.[84] Moreover, large molecules could passivate surface defects to fabricate high-efficiency tin-based PSCs.[85] However, the crystal growth pace of 2D perovskite is slower, and the transport properties are poorer than the 3D counterpart.[50] Thus, researchers combined the advantages of 2D and 3D structures in 2D/3D structures.

Li and co-workers[86] prepared 2D/3D structure $CsSnBrI_{2-x}(SCN)_x$ by introducing phenylethylamine hydroiodate (PEAI) and thiocyanate (SCN). Researching the crystal growth kinetics, they observed that PEAI and Sn(SCN) could form 2D structures acting as an intermediate template to induce 3D perovskite growth. By comparison, the effect of SCN⁻ addition, these films exhibit better out-of-plane orientation, and large grain sizes cause less defect density (**Figure 11**b). Besides, stable 2D structure perovskite as a surface layer could increase oxidation resistance. Later, Yu and co-workers[10b] reported a new strategy to use 4-fluoro-phenethylammonium bromide (FPEABr) instead of FAI to form 2D/3D $FASnI_3$. They achieved a PCE of 14.81% (14.01% certified) at a 10% addition of FPEABr. When the addition ratio is below 20%, FPEABr enhances the performance, forming a 2D phase that induces 3D highly oriented growth. However, this rule will be the opposite when the concentration is above 20%. At a low concentration regime of FPEABr, the 2D phase wrap-around 3D grains and locate itself at the surfaces and grain boundaries. This phenomenon prevents the oxidation of $Sn^{2+}$ and decreases the defect density. Recently, Sanchez–Diaz and co-workers[87] used a chemical engineering approach to prevent Sn perovskite degradation. They introduced dipropylammonium iodide (Dipl) and a reducing agent, sodium borohydride ($NaBH_4$), to form 2D/3D Sn-based PSCs. By studying the degradation mechanism of $FASnI_3$, they found that $I_2$ is released in light immersion conditions, and many defects are formed. The combination of Dipl and $NaBH_4$ could balance and fix surface iodine (Figure 11a). In addition, Dipl prevents $I_2$ migration to the surface, and $NaBH_4$ could assist Dipl. Thus, with the addition of Dipl and $NaBH_4$, the oxidation of $Sn^{2+}$ is reduced, and $FASnI_3$ stability is enhanced compared to the control device. This work reported devices with a PCE of over 10% and retained 96% of the initial PCE after 1300 h at MPP in $N_2$. More recently, Kang and groups found wide band gap perovskite with some problems such as instability. Thus, they explored the performance of wide band gap (1.6 eV) 2D/3D Sn perovskite $PEA_xFA_{0.75}MA_{0.25-x}SnI_2Br$ by introducing $PEA^+$. (Figure 11c) The composition of perovskite A-site cation is adjusted by component engineering. They found that the $PEA^+$ and $MA^+$ could remarkably reduce surface defects and improve film morphology (Figure 11d). A layer of 2D perovskite induced by $PEA^+$ was prepared on the 3D layer, preventing water and oxygen leakage and passing through grain boundaries. As a result, the film exhibited slow lifetime decay (1.25 ns) and increased charge extraction. Reduced trap state density ($1.7 \times 10^{16}$ cm$^{-3}$) and improved band alignment with slower carrier recombination ($\tau = 1217$ µs). As a new strategy for enhancing Sn perovskite's stability, the 2D/3D method is effective, could be rapidly developed, and is worthy of further research.[88]

In short, 2D/3D perovskite exhibit many superior characteristics which preserve the advantage of 3D structure and show the stability of 2D structure. 2D perovskite was grown on the surface of 3D structure, demonstrating an encapsulating effect to improve stability. Moreover, 2D/3D could take advantage of the RP, DJ, ACI structure in the use of organic space cations, leading to the performance could be adjusted to a much greater degree. Currently, the PCE of 2D/3D Sn perovskite has reached 14.81%, the highest PCE, proving excellent stability and photoelectric properties. The important previous works about quasi-2D ACI Pb-based and 2D/3D Sn-based PSCs were concluded in **Table 4**.

## 5. Conclusion and Outlook

In this review, we emphasized the key role of dimensional tuning in improving the quality of Sn-based perovskite films and the performance of their PSCs. We summarized the recent progress of three-dimensional and layered 2D tin-based perovskites, including RP, DJ, ACI, and 2D/3D. Many scientific research schemes were proposed on the stability of tin perovskites, from the initial $SnF_2$ additive to the formation of 2D structures. Surprisingly, these quasi-2D structures have developed rapidly in recent years. The efficiency has increased from 2.5% in the beginning to more than 14% in pure tin PSCs and more than 20% in lead-tin mixed PSCs with improved stability. This allows tin perovskites to be a potential replacement for lead perovskites. The main advantage of a 2D structure is that some hydrophobic materials can be added between inorganic slabs to improve stability. Besides, additive modification on perovskites is permitted. These all suppressed the oxidation of $Sn^{2+}$ to $Sn^{4+}$. However, the performance of Sn-based perovskites is worse than Pb-based perovskites. Although 2D has shown great potential, there are still many challenges to solve before replacing lead entirely, as follows:

I. For 3D tin perovskites, researchers should focus on suppressing the oxidation of $Sn^{2+}$, decreasing crystallization rate and passivation of interfacial defects for improving stability and high PCE for application. More only than that, the device structure is also a crucial factor. The appropriate ETL and HTL could promote band alignment for better carrier transmissions.

**Table 4.** Summary of quasi-2D alternating cation interlayer (ACI) Pb-based and 2D/3D Sn-based perovskite photovoltaic parameters.

| Device structure | Device parameter | | | | Stability | Strategy | | Ref. |
|---|---|---|---|---|---|---|---|---|
| | PCE [%] | $J_{SC}$ [mA cm$^{-2}$] | $V_{OC}$ [V] | FF [%] | | | | |
| FTO/PEDOT:PSS/ $GAMA_3Pb_3I_{10}$/PCBM/Al | 7.26 | 9.36 | 0.974 | 79.7 | / | GA | ACI+ Band engineering | 2017[22] |
| ITO/PEDOT:PSS/(GA) $(MA)_3Pb_3I_{10}$/PCBM/Li-F/Al | 16.65 | 20.75 | 1.08 | 74.52 | 80% of initial PCE 2400 h in $N_2$ | GA | ACI+ Crystal grown | 2019[80] |
| FTO/c-$TiO_2$/(GA)$(MA)_3Pb_3I_{10}$/ PCBM/Ag | 14.7 | 18.8 | 1.15 | 67.8 | 88% of initial PCE after 240 days in $N_2$ | DMSO:DMF = 1:10 | ACI+ Crystallization kinetics | 2019[38a] |
| FTO/c-$TiO_2$/(GA)$(MA)_3Pb_3I_{10}$/ Spiro-OMeTAD/Au | 18.48 | 22.26 | 1.14 | 72.67 | 5% decay after 131 days in the dark | MACI | ACI+ Crystal grown | 2019[81] |
| FTO/c-$TiO_2$/(GA)$(MA)_3Pb_3I_{10}$/ Spiro-OMeTAD/Au | 19.18 | 22.68 | 1.08 | 78.01 | 95% of initial PCEs after 123 days in $N_2$ | DMSO:DMF = 1:10 | Solvent engineering | 2021[82] |
| FTO/PEDOT:PSS/ $CsSnBrI_2$-PS/PCBM/BCP/Ag | 5.01 | 17.2 | 0.43 | 68.7 | 92% of initial PCE after 3 h 60 °C in $N_2$ | PEAI, $SCN^-$ | 2D/3D, Crystallization kinetics | 2021[86] |
| ITO/PEDOT:PSS/$FASnI_3$/ ICBA/BCP/Al | 14.81 | 24.91 | 0.84 | 70.76 | / | FPEABr | 2D/3D, Crystal grown | 2021[10] |
| ITO/PEDOT:PSS/$FASnI_3$/C60/ BCP/Ag | 10.61 | 22.13 | 0.656 | 73.11 | 96% of the initial PCE after 1300 h at MPP in $N_2$ | $NaBH_4$+ Dipl | 2D/3D, Crystal grown | 2022[87] |
| ITO/PEDOT:PSS/ $PEA_{0.15}FA_{0.75}MA_{0.1}SnI_2Br$ / PCBM/BCP/Ag | 7.96 | 16.89 | 0.67 | 70.36 | 1500 h without decay in $N_2$ | Wide band gap, $PEA^+$ | 2D/3D, Energy band engineering | 2022[88] |

II. Research on RP structure tin-based perovskite is relatively complete. The hydrophobic organic spacer cations form RP perovskite and exhibit superior stability to 3D perovskite. However, the existence of van der Waals forces and relatively poor transport are representative factors that affect the performance improvement of RP perovskites. Thus, researchers should concentrate on enhancing interactions between organic spacers to find new organic cations and adding transport-enhancing additives to achieve a higher-quality Sn perovskite film.

III. Benefits from shortened interlayer distances eliminated/reduced van der Waals gaps and enhanced DJ and ACI hydrogen bonds. These lead to better stability and carrier transport capability and are easier to form a pure DJ phase. Moreover, DJ structure could apply to Sn–Pb perovskite with more than 20% PCE and superior stability that is beneficial to developing tandem perovskite. It is more convenient to understand the property of the DJ structure.

IV. Since there are no reports on tin-based ACI perovskites, researchers could draw on lead-based studies to experiment with them. Besides, researchers should focus on designing new hydrophobic cations combined with additives and cations to develop 2D perovskite and 2D/3D mixture perovskite to suppress the oxidation of $Sn^{2+}$. Meanwhile, exploring new single-crystal synthesis methods to form stable 2D single-crystal perovskite for inducing the growth of 3D perovskite to improve the performance of Sn perovskite.

V. Controlling perovskite strain. The introduction of large-volume cations changes atomic stacking. This causes lattice strain with defect states increasing, changing perovskite band structure which impacts the width of the band gap, hole effective mass, and carrier mobility. Thus, reasonable control of perovskite strain achieves highly efficient and stable tin-based perovskite. In structure, a suitable cation radius supplies opportunities to reduce stress. Explore new strategies to fabricate films, such as optimization of the annealing process, the addition of a small ion radius, and interface regulation. Additionally, residual control environmental factors such as temperature, external electric field, and illumination will regulate perovskite strain to achieve high performance and stable tin-based perovskite.

We believe that through an in-depth understanding of the dimension tuning and affected film crystallization and suppressing Sn oxidation, and there will be a significant improvement in the structural stability of Sn-based perovskites, accelerating the rapid development of lead-free PSCs.

## Acknowledgements

The authors thank Helmholtz-Zentrum Berlin for funding. The authors acknowledge financial support from the Natural Science Foundation of China (No. 51903181). G.L. acknowledges China Scholarship Council (CSC) for the financial support (Grant No. 201906150131). G.L. and M.H.A. thank the support from the HyPerCells Joint Graduate School. This work has received funding from the European Research Council (ERC) under the European Union's Horizon 2020 research and innovation program (Grant agreement No. 804519).

Open access funding enabled and organized by Projekt DEAL.

## Conflict of Interest

The authors declare no conflict of interest.

## Keywords

lead-free, perovskite solar cells, quasi-2D, stability, tin perovskites

Received: December 12, 2022
Revised: January 8, 2023

---

[1] D. W. de Quilettes, S. M. Vorpahl, S. D. Stranks, H. Nagaoka, G. E. Eperon, M. E. Ziffer, H. J. Snaith, D. S. Ginger, *Science* **2015**, *348*, 683.

[2] a) L. Wang, H. Zhou, J. Hu, B. Huang, M. Sun, B. Dong, G. Zheng, Y. Huang, Y. Chen, L. Li, *Science* **2019**, *363*, 265; b) D. Ma, K. Lin, Y. Dong, H. Choubisa, A. H. Proppe, D. Wu, Y.-K. Wang, B. Chen, P. Li, J. Z. Fan, *Nature* **2021**, *599*, 594; c) Y.-H. Kim, S. Kim, A. Kakekhani, J. Park, J. Park, Y.-H. Lee, H. Xu, S. Nagane, R. B. Wexler, D.-H. Kim, *Nat. Photonics* **2021**, *15*, 148.

[3] a) F. Hao, C. C. Stoumpos, D. H. Cao, R. P. Chang, M. G. Kanatzidis, *Nat. Photonics* **2014**, *8*, 489; b) L. A. Muscarella, A. Dučinskas, M. Dankl, M. Andrzejewski, N. P. M. Casati, U. Rothlisberger, J. Maier, M. Graetzel, B. Ehrler, J. V. Milić, *Adv. Mater.* **2022**, 2108720.

[4] a) A. Kojima, K. Teshima, Y. Shirai, T. Miyasaka, *J. Am. Chem. Soc.* **2009**, *131*, 6050; b) M. Kim, J. Jeong, H. Lu, T. K. Lee, F. T. Eickemeyer, Y. Liu, I. W. Choi, S. J. Choi, Y. Jo, H.-B. Kim, *Science* **2022**, *375*, 302; c) R. Prasanna, A. Gold-Parker, T. Leijtens, B. Conings, A. Babayigit, H.-G. Boyen, M. F. Toney, M. D. McGehee, *J. Am. Chem. Soc.* **2017**, *139*, 11117; d) L. M. Herz, *ACS Energy Lett.* **2017**, *2*, 1539; e) W. Ke, C. C. Stoumpos, M. G. Kanatzidis, *Adv. Mater.* **2019**, *31*, 1803230; f) S. D. Stranks, G. E. Eperon, G. Grancini, C. Menelaou, M. J. Alcocer, T. Leijtens, L. M. Herz, A. Petrozza, H. J. Snaith, *Science* **2013**, *342*, 341; g) Z. Wang, Q. Lin, F. P. Chmiel, N. Sakai, L. M. Herz, H. J. Snaith, *Nat. Energy* **2017**, *2*, 17135; h) H. Oga, A. Saeki, Y. Ogomi, S. Hayase, S. Seki, *J. Am. Chem. Soc.* **2014**, *136*, 13818; i) I. Chung, B. Lee, J. He, R. P. Chang, M. G. Kanatzidis, *Nature* **2012**, *485*, 486; j) J. Wang, N. Wang, Y. Jin, J. Si, Z. K. Tan, H. Du, L. Cheng, X. Dai, S. Bai, H. He, *Adv. Mater.* **2015**, *27*, 2311.

[5] a) J. Li, H.-L. Cao, W.-B. Jiao, Q. Wang, M. Wei, I. Cantone, J. Lü, A. Abate, *Nat. Commun.* **2020**, *11*, 310; b) A. H. Slavney, T. Hu, A. M. Lindenberg, H. I. Karunadasa, *J. Am. Chem. Soc.* **2016**, *138*, 2138.

[6] a) B. W. Park, B. Philippe, X. Zhang, H. Rensmo, G. Boschloo, E. M. Johansson, *Adv. Mater.* **2015**, *27*, 6806; b) J. Pal, S. Manna, A. Mondal, S. Das, K. Adarsh, A. Nag, *Angew. Chem., Int. Ed.* **2017**, *129*, 14375; c) I. Kopacic, B. Friesenbichler, S. F. Hoefler, B. Kunert, H. Plank, T. Rath, G. Trimmel, *ACS Appl. Energy Mater.* **2018**, *1*, 343; d) Z. Shi, J. Guo, Y. Chen, Q. Li, Y. Pan, H. Zhang, Y. Xia, W. Huang, *Adv. Mater.* **2017**, *29*, 1605005; e) D. Cortecchia, H. A. Dewi, J. Yin, A. Bruno, S. Chen, T. Baikie, P. P. Boix, M. Grätzel, S. Mhaisalkar, C. Soci, *Inorg. Chem.* **2016**, *55*, 1044.

[7] a) G. Nasti, A. Abate, *Adv. Energy Mater.* **2020**, *10*, 1902467; b) L. Zhang, X. Pan, L. Liu, L. Ding, *J. Semicond.* **2022**, *43*, 030203.

[8] a) Z. Zhao, F. Gu, Y. Li, W. Sun, S. Ye, H. Rao, Z. Liu, Z. Bian, C. Huang, *Adv. Sci.* **2017**, *4*, 1700204; b) A. Filippetti, S. Kahmann, C. Caddeo, A. Mattoni, M. Saba, A. Bosin, M. Loi, *J. Mater. Chem.* **2021**, *9*, 11812.

[9] a) N. K. Noel, S. D. Stranks, A. Abate, C. Wehrenfennig, S. Guarnera, A.-A. Haghighirad, A. Sadhanala, G. E. Eperon,

S. K. Pathak, M. B. Johnston, *Energy Environ. Sci.* **2014**, *7*, 3061; b) X. Jiang, F. Wang, Q. Wei, H. Li, Y. Shang, W. Zhou, C. Wang, P. Cheng, Q. Chen, L. Chen, Z. Ning, *Nat. Commun.* **2020**, *11*, 1245.

[10] B. B. Yu, Z. Chen, Y. Zhu, Y. Wang, B. Han, G. Chen, X. Zhang, Z. Du, Z. He, *Adv. Mater.* **2021**, *33*, 2102055;

[11] a) M. Aldamasy, Z. Iqbal, G. Li, J. Pascual, F. Alharthi, A. Abate, M. Li, *Phys. Chem. Chem. Phys.* **2021**, *23*, 23413; b) X. Liu, K. Yan, D. Tan, X. Liang, H. Zhang, W. Huang, *ACS Energy Lett.* **2018**, *3*, 2701; c) S. Shao, J. Liu, G. Portale, H.-H. Fang, G. R. Blake, G. H. ten Brink, L. J. A. Koster, M. A. Loi, *Adv. Energy Mater.* **2018**, *8*, 1702019; d) B. Ding, Y. Li, S.-Y. Huang, Q.-Q. Chu, C.-X. Li, C.-J. Li, G.-J. Yang, *J. Mater. Chem. A* **2017**, *5*, 6840.

[12] E. W.-G. Diau, E. Jokar, M. Rameez, *ACS Energy Lett.* **2019**, *4*, 1930.

[13] a) D. Di Girolamo, J. Pascual, M. H. Aldamasy, Z. Iqbal, G. Li, E. Radicchi, M. Li, S.-H. Turren-Cruz, G. Nasti, A. Dallmann, *ACS Energy Lett.* **2021**, *6*, 959; b) S. Wang, L. Yan, W. Zhu, Z. Cao, L. Zhou, L. Ding, F. Hao, *Nano Energy* **2022**, *99*, 107416; c) S. Wang, X. Zhang, W. Zhu, Z. Tang, J. Liu, H. Zhang, L. Ding, F. Hao, *Appl. Surf. Sci.* **2022**, *602*, 154393.

[14] a) W. Liao, D. Zhao, Y. Yu, C. R. Grice, C. Wang, A. J. Cimaroli, P. Schulz, W. Meng, K. Zhu, R. G. Xiong, *Adv. Mater.* **2016**, *28*, 9333; b) T.-B. Song, T. Yokoyama, S. Aramaki, M. G. Kanatzidis, *ACS Energy Lett.* **2017**, *2*, 897; c) F. Gu, S. Ye, Z. Zhao, H. Rao, Z. Liu, Z. Bian, C. Huang, *Solar RRL* **2018**, *2*, 1800136; d) F. Hao, C. C. Stoumpos, P. Guo, N. Zhou, T. J. Marks, R. P. Chang, M. G. Kanatzidis, *J. Am. Chem. Soc.* **2015**, *137*, 11445; e) T. C.-J. Yang, P. Fiala, Q. Jeangros, C. Ballif, *Joule* **2018**, *2*, 1421.

[15] C. Gai, J. Wang, Y. Wang, J. Li, *Energies* **2019**, *13*, 2.

[16] a) Y. Chen, Y. Sun, J. Peng, J. Tang, K. Zheng, Z. Liang, *Adv. Mater.* **2018**, *30*, 1703487; b) I. C. Smith, E. T. Hoke, D. Solis-Ibarra, M. D. McGehee, H. I. Karunadasa, *Angew. Chem., Int. Ed.* **2014**, *53*, 11232; c) L. Dou, *J. Mater. Chem.* **2017**, *5*, 11165.

[17] a) Z. Huang, A. H. Proppe, H. Tan, M. I. Saidaminov, F. Tan, A. Mei, C.-S. Tan, M. Wei, Y. Hou, H. Han, *ACS Energy Lett.* **2019**, *4*, 1521; b) H. Yao, W. Zhu, J. Hu, C. Wu, S. Wang, X. Zhao, X. Niu, L. Ding, F. Hao, *Chem. Eng. J.* **2023**, *455*, 140862.

[18] S. Ahmad, P. Fu, S. Yu, Q. Yang, X. Liu, X. Wang, X. Wang, X. Guo, C. Li, *Joule* **2019**, *3*, 794.

[19] P. Li, C. Liang, X. L. Liu, F. Li, Y. Zhang, X. T. Liu, H. Gu, X. Hu, G. Xing, X. Tao, *Adv. Mater.* **2019**, *31*, 1901966.

[20] L. Yan, J. Ma, P. Li, S. Zang, L. Han, Y. Zhang, Y. Song, *Adv. Mater.* **2022**, *34*, 2106822.

[21] N. Mercier, *Angew. Chem., Int. Ed.* **2019**, *58*, 17912.

[22] C. M. M. Soe, C. C. Stoumpos, M. Kepenekian, B. Traoré, H. Tsai, W. Nie, B. Wang, C. Katan, R. Seshadri, A. D. Mohite, *J. Am. Chem. Soc.* **2017**, *139*, 16297.

[23] Z. Xiao, W. Meng, B. Saparov, H.-S. Duan, C. Wang, C. Feng, W. Liao, W. Ke, D. Zhao, J. Wang, *J. Phys. Chem. Lett.* **2016**, *7*, 1213.

[24] J. Wang, J. Dong, F. Lu, C. Sun, Q. Zhang, N. Wang, *J. Mater. Chem.* **2019**, *7*, 23563.

[25] D. H. Cao, C. C. Stoumpos, O. K. Farha, J. T. Hupp, M. G. Kanatzidis, *J. Am. Chem. Soc.* **2015**, *137*, 7843.

[26] a) H. Tsai, W. Nie, J.-C. Blancon, C. C. Stoumpos, R. Asadpour, B. Harutyunyan, A. J. Neukirch, R. Verduzco, J. J. Crochet, S. Tretiak, *Nature* **2016**, *536*, 312; b) H. Ren, S. Yu, L. Chao, Y. Xia, Y. Sun, S. Zuo, F. Li, T. Niu, Y. Yang, H. Ju, *Nat. Photonics* **2020**, *14*, 154.

[27] S. Kahmann, S. Shao, M. A. Loi, *Adv. Funct. Mater.* **2019**, *29*, 1902963.

[28] C. C. Stoumpos, C. D. Malliakas, M. G. Kanatzidis, *Inorg. Chem.* **2013**, *52*, 9019.

[29] L. Ma, F. Hao, C. C. Stoumpos, B. T. Phelan, M. R. Wasielewski, M. G. Kanatzidis, *J. Am. Chem. Soc.* **2016**, *138*, 14750.

[30] a) H. Hu, B. Dong, W. Zhang, *J. Mater. Chem. A* **2017**, *5*, 11436; b) H.-H. Fang, S. Adjokatse, S. Shao, J. Even, M. A. Loi, *Nat. Commun.* **2018**, *9*, 243; c) W. Li, Z. Wang, F. Deschler, S. Gao, R. H. Friend, A. K. Cheetham, *Nat. Rev. Mater.* **2017**, *2*, 16099.

[31] a) J. Liu, M. Ozaki, S. Yakumaru, T. Handa, R. Nishikubo, Y. Kanemitsu, A. Saeki, Y. Murata, R. Murdey, A. Wakamiya, *Angew. Chem., Int. Ed.* **2018**, *130*, 13405; b) T. Yokoyama, D. H. Cao, C. C. Stoumpos, T.-B. Song, Y. Sato, S. Aramaki, M. G. Kanatzidis, *J. Phys. Chem. Lett.* **2016**, *7*, 776.

[32] a) E. Jokar, C.-H. Chien, A. Fathi, M. Rameez, Y.-H. Chang, E. W.-G. Diau, *Energy Environ. Sci.* **2018**, *11*, 2353; b) T. Wu, X. Liu, X. He, Y. Wang, X. Meng, T. Noda, X. Yang, L. Han, *Sci. China Chem.* **2019**, *63*, 107.

[33] A. Aftab, M. I. Ahmad, *Sol. Energy* **2021**, *216*, 26.

[34] B. Wu, Y. Zhou, G. Xing, Q. Xu, H. F. Garces, A. Solanki, T. W. Goh, N. P. Padture, T. C. Sum, *Adv. Funct. Mater.* **2017**, *27*, 1604818.

[35] M. Li, F. Li, J. Gong, T. Zhang, F. Gao, W.-H. Zhang, M. Liu, *Small Struct.* **2022**, *3*, 2100102.

[36] S. Zhang, P. Audebert, Y. Wei, A. Al Choueiry, G. Lanty, A. Bréhier, L. Galmiche, G. Clavier, C. Boissiere, J.-S. Lauret, *Materials* **2010**, *3*, 3385.

[37] M. Wang, Y. Li, X. Zhao, W. Wang, J. Chen, W. Zhang, Y. Huang, L. Zhang, S. Chen, *Sol. RRL* **2022**, *6*, 2100800.

[38] a) Y. Zhang, P. Wang, M.-C. Tang, D. Barrit, W. Ke, J. Liu, T. Luo, Y. Liu, T. Niu, D.-M. Smilgies, *J. Am. Chem. Soc.* **2019**, *141*, 2684; b) J. Gong, M. Hao, Y. Zhang, M. Liu, Y. Zhou, *Angew. Chem., Int. Ed.* **2022**, *61*, e202112022.

[39] P. Cheng, Z. Xu, J. Li, Y. Liu, Y. Fan, L. Yu, D.-M. Smilgies, C. Müller, K. Zhao, S. F. Liu, *ACS Energy Lett.* **2018**, *3*, 1975.

[40] C. Ma, D. Shen, T. W. Ng, M. F. Lo, C. S. Lee, *Adv. Mater.* **2018**, *30*, 1800710.

[41] A. v. Bondi, *J. Phys. Chem.* **1964**, *68*, 441.

[42] D. Ghosh, D. Acharya, L. Pedesseau, C. Katan, J. Even, S. Tretiak, A. J. Neukirch, *J. Mater. Chem.* **2020**, *8*, 22009.

[43] W. Ke, L. Mao, C. C. Stoumpos, J. Hoffman, I. Spanopoulos, A. D. Mohite, M. G. Kanatzidis, *Adv. Energy Mater.* **2019**, *9*, 1803384.

[44] L. Mao, W. Ke, L. Pedesseau, Y. Wu, C. Katan, J. Even, M. R. Wasielewski, C. C. Stoumpos, M. G. Kanatzidis, *J. Am. Chem. Soc.* **2018**, *140*, 3775.

[45] a) Y. Chen, S. Yu, Y. Sun, Z. Liang, *J. Phys. Chem. Lett.* **2018**, *9*, 2627; b) G. Liu, Z. Liu, F. Zeng, X. Wang, S. Li, X. Xie, *Chem. Phys. Lett.* **2020**, *743*, 137186.

[46] Y. Xu, M. Wang, Y. Lei, Z. Ci, Z. Jin, *Adv. Energy Mater.* **2020**, *10*, 2002558.

[47] J. Shi, Y. Gao, X. Gao, Y. Zhang, J. Zhang, X. Jing, M. Shao, *Adv. Mater.* **2019**, *31*, 1901673.

[48] D. H. Cao, C. C. Stoumpos, T. Yokoyama, J. L. Logsdon, T.-B. Song, O. K. Farha, M. R. Wasielewski, J. T. Hupp, M. G. Kanatzidis, *ACS Energy Lett.* **2017**, *2*, 982.

[49] I. Zimmermann, S. Aghazada, M. K. Nazeeruddin, *Angew. Chem., Int. Ed.* **2019**, *131*, 1084.

[50] J. Qiu, Y. Xia, Y. Chen, W. Huang, *Adv. Sci.* **2019**, *6*, 1800793.

[51] G. Li, Z. Su, M. Li, F. Yang, M. H. Aldamasy, J. Pascual, F. Yang, H. Liu, W. Zuo, D. Di Girolamo, *Adv. Energy Mater.* **2021**, *11*, 2101539.

[52] F. Li, Y. Xie, Y. Hu, M. Long, Y. Zhang, J. Xu, M. Qin, X. Lu, M. Liu, *ACS Energy Lett.* **2020**, *5*, 1422.

[53] X. Zhang, G. Wu, W. Fu, M. Qin, W. Yang, J. Yan, Z. Zhang, X. Lu, H. Chen, *Adv. Energy Mater.* **2018**, *8*, 1702498.

[54] Y. Liao, H. Liu, W. Zhou, D. Yang, Y. Shang, Z. Shi, B. Li, X. Jiang, L. Zhang, L. N. Quan, *J. Am. Chem. Soc.* **2017**, *139*, 6693.

[55] K. Chen, P. Wu, W. Yang, R. Su, D. Luo, X. Yang, Y. Tu, R. Zhu, Q. Gong, *Nano Energy* **2018**, *49*, 411.

[56] Y. Liu, M. Bag, L. A. Renna, Z. A. Page, P. Kim, T. Emrick, D. Venkataraman, T. P. Russell, *Adv. Energy Mater.* **2016**, *6*, 1501606.

[57] M. Liao, B. B. Yu, Z. Jin, W. Chen, Y. Zhu, X. Zhang, W. Yao, T. Duan, I. Djerdj, Z. He, *ChemSusChem* **2019**, *12*, 5007.

[58] M. Li, W.-W. Zuo, Y.-G. Yang, M. Aldamasy, Q. Wang, S. H. T. Cruz, S.-L. Feng, M. Saliba, Z.-K. Wang, A. Abate, *ACS Energy Lett.* **2020**, *5*, 1923.
[59] X. Jiang, H. Li, Q. Zhou, Q. Wei, M. Wei, L. Jiang, Z. Wang, Z. Peng, F. Wang, Z. Zang, *J. Am. Chem. Soc.* **2021**, *143*, 10970.
[60] J. Qiu, Y. Xia, Y. Zheng, W. Hui, H. Gu, W. Yuan, H. Yu, L. Chao, T. Niu, Y. Yang, *ACS Energy Lett.* **2019**, *4*, 1513.
[61] J. Qiu, Y. Lin, X. Ran, Q. Wei, X. Gao, Y. Xia, P. Müller-Buschbaum, Y. Chen, *Sci. China Chem.* **2021**, *64*, 1577.
[62] a) H. Xu, Y. Jiang, T. He, S. Li, H. Wang, Y. Chen, M. Yuan, J. Chen, *Adv. Funct. Mater.* **2019**, *29*, 1807696; b) A. Mei, X. Li, L. Liu, Z. Ku, T. Liu, Y. Rong, M. Xu, M. Hu, J. Chen, Y. Yang, *Science* **2014**, *345*, 295.
[63] G. Grancini, C. Roldán-Carmona, I. Zimmermann, E. Mosconi, X. Lee, D. Martineau, S. Narbey, F. Oswald, F. De Angelis, M. Graetzel, *Nat. Commun.* **2017**, *8*, 15684.
[64] N. Sun, W. Gao, H. Dong, X. Liu, L. Chao, W. Hui, Y. Xia, C. Ran, Y. Chen, *ACS Appl. Energy Mater.* **2022**, *5*, 4008.
[65] Y. Xu, K.-J. Jiang, P. Wang, W.-M. Gu, G.-H. Yu, X. Zhou, Y. Song, *New J. Chem.* **2022**, *46*, 2259.
[66] H. Wu, X. Lian, J. Li, Y. Zhang, G. Zhou, X. Wen, Z. Xie, H. Zhu, G. Wu, H. Chen, *J. Mater. Chem. A* **2021**, *9*, 12566.
[67] a) X. Zhao, T. Liu, A. B. Kaplan, C. Yao, Y.-L. Loo, *Nano Lett.* **2020**, *20*, 8880; b) Z. Xu, D. Lu, X. Dong, M. Chen, Q. Fu, Y. Liu, *Adv. Mater.* **2021**, *33*, 2105083.
[68] a) B. Saparov, D. B. Mitzi, *Chem. Rev.* **2016**, *116*, 4558; b) H. Lai, D. Lu, Z. Xu, N. Zheng, Z. Xie, Y. Liu, *Adv. Mater.* **2020**, *32*, 2001470.
[69] X. Lian, H. Wu, L. Zuo, G. Zhou, X. Wen, Y. Zhang, G. Wu, Z. Xie, H. Zhu, H. Chen, *Adv. Funct. Mater.* **2020**, *30*, 2004188.
[70] P. Huang, S. Kazim, M. Wang, S. Ahmad, *ACS Energy Lett.* **2019**, *4*, 2960.
[71] a) Z. Shi, Z. Ni, J. Huang, *ACS Energy Lett.* **2022**, *7*, 984; b) J. Hu, I. W. Oswald, S. J. Stuard, M. M. Nahid, N. Zhou, O. F. Williams, Z. Guo, L. Yan, H. Hu, Z. Chen, X. Xiao, Y. Lin, Z. Yang, J. Huang, A. M. Moran, H. Ade, J. R. Neilson, W. You, *Nat. Commun.* **2019**, *10*, 1276; c) X. Li, W. Ke, B. Traoré, P. Guo, I. Hadar, M. Kepenekian, J. Even, C. Katan, C. C. Stoumpos, R. D. Schaller, *J. Am. Chem. Soc.* **2019**, *141*, 12880.
[72] F. Zhang, S. Y. Park, C. Yao, H. Lu, S. P. Dunfield, C. Xiao, S. Uličná, X. Zhao, L. Du Hill, X. Chen, *Science* **2022**, *375*, 71.
[73] L. Cheng, Z. Liu, S. Li, Y. Zhai, X. Wang, Z. Qiao, Q. Xu, K. Meng, Z. Zhu, G. Chen, *Angew. Chem., Int. Ed.* **2021**, *60*, 856.
[74] M. Chen, M.-G. Ju, M. Hu, Z. Dai, Y. Hu, Y. Rong, H. Han, X. C. Zeng, Y. Zhou, N. P. Padture, *ACS Energy Lett.* **2018**, *4*, 276.
[75] M. Chen, Q. Dong, F. T. Eickemeyer, Y. Liu, Z. Dai, A. D. Carl, B. Bahrami, A. H. Chowdhury, R. L. Grimm, Y. Shi, *ACS Energy Lett.* **2020**, *5*, 2223.
[76] P. Li, X. Liu, Y. Zhang, C. Liang, G. Chen, F. Li, M. Su, G. Xing, X. Tao, Y. Song, *Angew. Chem., Int. Ed.* **2020**, *132*, 6976.
[77] B. Ma, J. Chen, M. Wang, X. Xu, J. Qian, Y. Lu, W. Zhang, P. Xia, M. Qin, W. Zhu, *J. Phys. Chem. C* **2020**, *124*, 16289.
[78] W. Ke, C. Chen, I. Spanopoulos, L. Mao, I. Hadar, X. Li, J. M. Hoffman, Z. Song, Y. Yan, M. G. Kanatzidis, *J. Am. Chem. Soc.* **2020**, *142*, 15049.
[79] J. Cao, F. Yan, *Energy Environ. Sci.* **2021**, *14*, 1286.
[80] H. Gu, C. Liang, Y. Xia, Q. Wei, T. Liu, Y. Yang, W. Hui, H. Chen, T. Niu, L. Chao, *Nano Energy* **2019**, *65*, 104050.
[81] T. Luo, Y. Zhang, Z. Xu, T. Niu, J. Wen, J. Lu, S. Jin, S. Liu, K. Zhao, *Adv. Mater.* **2019**, *31*, 1903848.
[82] J. Yang, T. Yang, D. Liu, Y. Zhang, T. Luo, J. Lu, J. Fang, J. Wen, Z. Deng, S. Liu, *Sol. RRL* **2021**, *5*, 2100286.
[83] C. Hanmandlu, A. Singh, K. M. Boopathi, C.-S. Lai, C.-W. Chu, *Rep. Prog. Phys.* **2020**, *83*, 086502.
[84] B. Kim, S. I. Seok, *Energy Environ. Sci.* **2020**, *13*, 805.
[85] J.-W. Lee, Z. Dai, T.-H. Han, C. Choi, S.-Y. Chang, S.-J. Lee, N. De Marco, H. Zhao, P. Sun, Y. Huang, Y. Yang, *Nat. Commun.* **2018**, *9*, 3201.
[86] H. Li, X. Jiang, Q. Wei, Z. Zang, M. Ma, F. Wang, W. Zhou, Z. Ning, *Angew. Chem., Int. Ed.* **2021**, *133*, 16466.
[87] J. Sanchez-Diaz, R. S. Sánchez, S. Masi, M. Krecĉmarová, A. O. Alvarez, E. M. Barea, J. Rodriguez-Romero, V. S. Chirvony, J. F. Sánchez-Royo, J. P. Martinez-Pastor, *Joule* **2022**, *6*, 861.
[88] S. Cho, P. Pandey, J. Park, T.-W. Lee, H. Ahn, H. Choi, D.-W. Kang, *Chem. Eng. J.* **2022**, *446*, 137388.

**Jinbo Zhao** received his B.S. degree in function materials from the Henan Normal University in 2021. Currently, he is pursuing a master's degree in materials science and engineering at the Key Lab for Special Functional Materials of Ministry of Education, Henan University. And he mainly focuses on the stability of organic–inorganic hybrid perovskite solar cells (PSCs) at present.

**Zuhong Zhang** received his master's degree in materials science and engineering under the supervision of Dr. Hairui Liu from Henan Normal University in July 2021. Currently, he is pursuing a PhD degree in physics at the Key Lab for Special Functional Materials of Ministry of Education, Henan University. And he mainly focuses on the stability of organic-inorganic hybrid perovskite solar cells (PSCs) at present.

**Guixiang Li** is a doctoral researcher at Helmholtz-Zentrum Berlin für Materialien und Energie (HZB). He received his master degree in Green Energy Chemistry and Technology from South China University of Technology (SCUT) in 2019. Guixiang's current research includes processing high-quality lead-free tin-based perovskite materials and crystallization dynamics of halide perovskites for efficient photovoltaics.

**Mahmoud Aldamasy** received his M.Phil. degree in Physical Chemistry from Zagazig University, Egypt. He has been working at Egyptian petroleum research institute (EPRI) on petroleum applications and was a visiting PhD researcher at Kyoto University. He is now a DAAD PhD scholar at Helmholtz Center Berlin for Energy and Materials and working on finding new solvents for tin perovskites at the department of novel materials and interfaces for photovoltaic solar cells.

**Meng Li** obtained his Ph.D. degree in materials science and engineering under the supervision of Prof. Liang-Sheng Liao from Soochow University in Jun. 2018. He pursued his postdoctoral research in the Helmholtz-Zentrum Berlin für Materialien und Energie (HZB) from Oct 2018 to Sep 2021. Currently, he has joined the Key Lab for Special Functional Materials of Ministry of Education, Henan University. And Dr. Li mainly focuses on organic–inorganic hybrid materials for optoelectronic applications at present. His main research interests lie in the application of nontoxic photovoltaic materials and devices.

**Antonio Abate** is team leader at the Helmholtz-Centrum Berlin and tenure track professor at University of Naples Federico II. He is researching solar energy conversion with perovskite solar cells (PSCs). Before the current position, Antonio was leading the solar cell research at the University of Fribourg in Switzerland. He was a Marie SkłodowskaCurie Fellow at École Polytechnique Fédérale de Lausanne. He worked for 4 years as a postdoctoral researcher at the University of Oxford and the University of Cambridge. Antonio graduated from University of Naples Federico II in 2006, and he got his PhD at Politecnico di Milano in 2011.